Axisymmetric Rocket Nozzle Design

Jason Etele
Institute for Aerospace Studies, University of Toronto

Written in November 2001

jason.etele@utoronto.ca
Document generated on July 29, 2015.

WARP
Weakly-ionized Airflow Resolver & Post-processor

Contents

1 Introduction

This document contains a methodology that can be used to design an axisymmetric rocket nozzle. The design method incorporates such variables as *(a)* fuel/oxidizer combination used in the combustion chamber, *(b)* desired Mach number at the nozzle exit plane, and *(c)* viscous effects.

The combustion process is modeled assuming equilibrium combustion at constant pressure using the Gibbs Minimization Technique. The post combustion mixture properties (species mass fractions, specific heat ratio, etc.) are then used as the input conditions for a converging/diverging supersonic nozzle which assumes frozen flow throughout the expansion process. The converging nozzle section is based on an algebraic expression while the diverging contour is designed such that a specific Mach number distribution along the nozzle centreline is obtained. This specific contour is found using the two-dimensional method of characteristics.

The beginning of this document contains a brief description of the theory used in the design process while the remaining sections contain examples of the theory applied to several cases of interest. The entire set of input variables required for a complete nozzle design are listed in Table 1.

2 Combustion Chamber Theory

This section outlines a method that can be used to calculate the chemical composition of a post combustion mixture based on the assumption of achieving chemical equilibrium. This assumption goes one step further than the basic complete combustion assumption from which stoichiometric ratios are calculated, but still lies one step short of accounting for the complete combustion scenario. Equilibrium combustion allows for the fact that species other than those found in the complete combustion case can be present in the post combustion mixture (i.e. dissociated products, incomplete combustion products, etc.) but does not take into account the time rate of change of these species. Thus it is the non-equilibrium combustion process carried through sufficient time to allow chemical equilibrium to be achieved (or thought of another

TABLE 1.
Rocket Nozzle Design Parameters

Design Variable	Typical Values
Fuel	Kerosene ($C_{12}H_{24}$), Hydrogen (H_2)
Oxidizer	Air (79% N_2, 21% O_2), Oxygen (O_2)
Equivalence Ratio	0.1 - 3.0
Fuel Input Temperature	300 - 1,000 K
Total Pressure	1 - 10 MPa
Exit Mach Number	1.5 - 6.0
Maximum Expansion Angle	10 - 15 degrees
Throat Height	5 - 50 mm
Viscosity	Yes/No
Nozzle Wall Temperature	500 - 1000 K
Mach Number at Combustion Chamber Exit	0.001 - 0.1
Subsonic Nozzle Section Length (% of Supersonic Length)	15% - 45%

way, it is the non-equilibrium combustion process assuming infinite reaction rates). There are two major methods for calculating chemical equilibrium mixtures, the Equilibrium Constant Method and the Gibbs Minimization Method, the latter of which is described here.

2.1 Gibbs Minimization Technique

The major attraction of the Gibbs Minimization Technique for solving chemical equilibrium over the more traditional Equilibrium Constant Method is that the system of equations obtained from the Gibbs method is usually easier to solve than that for the Equilibrium Constant method. In the Equilibrium Constant Method one is required to define n distinct chemical reactions (where n is equal to the total number of species to be considered, n_s, minus 2) which along with Dalton's Law of partial pressures and the fact that the ratio of fuel atoms to oxidizer atoms is constant (in the absence of nuclear reactions) yields a system of n equations to be solved simultaneously. The drawback of this approach is that due to the nature of the equilibrium constant, the system of equations is normally non-linear and hence very difficult to solve.

However the Gibbs Minimization Technique, although perhaps less intuitive and slightly more complex in its derivation, results in a system of only $n_a + 2$ equations (where n_a is the total number of distinct atomic particles involved in the reaction, which for the case of most hydrocarbon fuels is 4 [C, H, N, O]). As well as significantly reducing the number of equations that need to be solved, this approach also results in a linear system of equations allowing for a much simpler solution process.

Starting first by defining the Gibbs energy of a species k,

$$g_k = h_k - Ts_k = h_k^o - Ts_k^o + \overline{R}T\ln(\frac{\sigma_k}{\sigma_m}) + \overline{R}T\ln(\frac{p}{p^o}) \tag{1}$$

where h_k and s_k are the enthalpy and entropy of species k respectively at the temperature T (assuming that the species is being considered on its own). However, since in most cases these values are found via experimentally determined polynomials which are functions of T taken at a particular reference pressure p^o (usually 1 atm = 101325 Pa), the values h_k^o and s_k^o can be used if the term in Eq. 1 involving the actual pressure, p (which must be in units of atm), is added. Also, to consider a species k which is part of a mixture of other species, the remaining term in Eq. 1 involving the species kmols, σ_k, and the total kmols of the entire mixture, σ_m, is needed to account for the energy available through the expansion of species k from its partial pressure in the mixture to the ambient pressure of the mixture as a whole. Note that Eq. 1 yields the Gibbs energy in units of [J/kmol] when the units of the Universal Gas Constant, $\overline{R}$, are 8314.3 [J/kmol K].

Having established the Gibbs energy of an individual species within a mixture on a molar basis, the Gibbs energy of the entire mixture can be written as,

$$G = \sum_{k=0}^{k=\overline{n_s}} \sigma_k g_k \tag{2}$$

where $\overline{n_s}$ is the total number of species being considered, n_s, minus 1 (since the index starts at zero). As the name of the method implies, finding the equilibrium composition involves taking the derivative of the Gibbs energy (Eq. 2) with respect to each species under consideration and setting this equal to zero (hence minimizing the Gibbs function),

$$dG = \sum_{j=0}^{j=\overline{n_s}} \frac{\partial G}{\partial \sigma_j} d\sigma_j = 0$$

which is a condition for a mixture in chemical equilibrium. Substituting the definition of total Gibbs energy (Eqs. 1 and 2) into the above while multiplying out the sum over k, defining a reference Gibbs energy as

$$g_k^o = h_k^o - T s_k^o \tag{3}$$

and realizing that the total kmols is simply the sum of the individual species kmols,

$$\sigma_m = \sum_{i=0}^{i=\overline{n_s}} \sigma_i \tag{4}$$

one can write,

$$dG = \sum_{j=0}^{j=\overline{n_s}} \frac{\partial}{\partial \sigma_j} \left\{ \sum_{k=0}^{k=\overline{n_s}} \sigma_k g_k^o + \sum_{k=0}^{k=\overline{n_s}} \sigma_k \overline{R} T \ln(\sigma_k) - \sum_{k=0}^{k=\overline{n_s}} \sigma_k \overline{R} T \ln\left(\sum_{i=0}^{i=\overline{n_s}} \sigma_i\right) + \sum_{k=0}^{k=\overline{n_s}} \sigma_k \overline{R} T \ln\left(\frac{p}{p^o}\right) \right\} d\sigma_j = 0$$

After evaluating the derivative above, the familiar form of the chemical equilibrium condition can be obtained,

$$\boxed{dG = \textstyle\sum_{k=0}^{k=\overline{n_s}} g_k d\sigma_k = 0} \tag{5}$$

As well as specifying the minimization of the Gibbs energy at equilibrium, one can also make use of the fact that although there are n_s species, each of these is composed of ratios of elementary particles, of which there are far fewer. Thus no matter how many species are considered (representing numerous chemical reactions) the total number of elementary atoms must remain constant. Expressing this relation mathematically,

$$\boxed{\textstyle\sum_{k=0}^{k=\overline{n_s}} \eta_{ik} \sigma_k = b_i^*; \qquad i = 0 \rightarrow \overline{n_a}} \tag{6}$$

where η_{ik} is the number of kg-atoms of i per kmol of species k (e.g. for O_2 $\eta = 2$) and b_i^* is the total number of kg-atoms of atom i. The index i goes from 0 to $\overline{n_a}$ where $\overline{n_a}$ is the total number of distinct atoms, n_a, minus 1.

Another constraint equation can be derived from the fact that total energy must also be conserved, which for the case of an adiabatic reaction yields,

$$\boxed{\textstyle\sum_{k=0}^{k=\overline{n_s}} h_k \sigma_k = H^*} \tag{7}$$

which is simply an equation expressing the conservation of total enthalpy during the combustion process. Note here that h_k is the enthalpy of species k per kmol of species k while H^* is the total enthalpy of the entire mixture (assuming negligible velocity within the combustion chamber).

Going back to Eq. 6, taking its derivative with respect to σ_k and multiplying each i equation by a constant λ_i one gets,

$$\lambda_i \left\{ \sum_{k=0}^{k=\overline{n_s}} \eta_{ik} d\sigma_k \right\} = 0 \qquad i = 0 \rightarrow \overline{n_a}$$

since the total number of atoms of each type is a constant throughout combustion. Adding the above result to Eq. 5 yields,

$$\lambda_0 \sum_{k=0}^{k=\overline{n_s}} \eta_{0k} d\sigma_k + \lambda_1 \sum_{k=0}^{k=\overline{n_s}} \eta_{1k} d\sigma_k + \ldots + \lambda_{\overline{n_a}} \sum_{k=0}^{k=\overline{n_s}} \eta_{\overline{n_a}k} d\sigma_k + \sum_{k=0}^{k=\overline{n_s}} g_k d\sigma_k = 0$$

which after some manipulation can be reduced to,

$$\boxed{g_k + \textstyle\sum_{i=0}^{i=\overline{n_a}} \lambda_i \eta_{ik} = 0 \qquad\qquad k = 0 \rightarrow \overline{n_s}} \tag{8}$$

At this point one must decide on a solution method for the equations derived above. Choosing a Newton-Raphson system of correction equations for which there are n number of correction variables Δx_j one can write (for the general functional f_s),

$$\sum_{j=1}^{j=n} \frac{\partial f_s}{\partial x_j} \Delta x_j = -f_s \tag{9}$$

Putting Eq. 6 into this form yields,

$$f_s = f_i = \sum_{k=0}^{k=\overline{n_s}} \eta_{ik} \sigma_k - b_i^* \qquad\qquad i = 0 \rightarrow \overline{n_a} \tag{10}$$

while the conservation of enthalpy equation (Eq. 7) can be expressed in this form as (dividing by $\overline{R}T$ as well),

$$f_s = f_T = \sum_{k=0}^{k=\overline{n_s}} \frac{h_k}{\overline{R}T} \sigma_k - \frac{H^*}{\overline{R}T} \tag{11}$$

If one chooses to define a non-dimensional Lagrange multiplier,

$$\pi_i = -\frac{\lambda_i}{\overline{R}T} \tag{12}$$

then one can also phrase each of the $\overline{n_s}$ equations in Eq. 8 as

$$f_s = f_k = \frac{g_k}{\overline{R}T} - \sum_{i=0}^{i=\overline{n_a}} \pi_i \eta_{ik} \qquad\qquad k = 0 \rightarrow \overline{n_s} \tag{13}$$

As a final step, one can also define a constraint equation based on the fact that the individual kmols of each species k must sum to the total kmols of the mixture,

$$f_s = f_m = \sum_{k=0}^{k=\overline{n_s}} \sigma_k - \sigma_m \tag{14}$$

(Aside: Lagrange multipliers are used when one wishes to find the extreme values of a function [either the maximum or minimum values] subject to certain side constraints. Thus in this case, one is trying to obtain the minimum value of the Gibbs energy subject to the side constraints of (a) conservation of total enthalpy (b) conservation of the total number of atoms and (c) ensuring the sum of the kmols of each species equals the independently determined total kmols of mixture.)

Having defined the desired functionals, the next step is to define the correction variables to be used. In this case, by judicious choice of these values one can simplify the resulting system of equations to be solved. If one chooses $\Delta \ln(\sigma_k)$ ($k = 0 \rightarrow \overline{n_s}$), $\Delta \ln(\sigma_m)$, and $\Delta \ln(T)$ then the Newton-Raphson scheme in Eq. 9 can be written for a general functional f_s as,

$$\boxed{\textstyle\sum_{k=0}^{k=ns} \frac{\partial f_s}{\partial \ln(\sigma_k)} \Delta \ln(\sigma_k) + \frac{\partial f_s}{\partial \ln(\sigma_m)} \Delta \ln(\sigma_m) + \frac{\partial f_s}{\partial \ln(T)} \Delta \ln(T) = -f_s} \tag{15}$$

Starting first with Eq. 13 (which itself is actually n_s equations) and taking the required derivatives will allow its substitution into Eq. 15 (this process will be shown for this functional, while only the final results will be shown for the remaining variables). Substituting the index j for k to avoid confusion one can write,

$$f_j = \frac{g_j}{\overline{R}T} - \sum_{i=0}^{i=\overline{n_a}} \pi_i \eta_{ij} \qquad j = 0 \rightarrow \overline{n_s}$$

which when replacing g_j with Eqs. 1 and 3 yields,

$$f_j = \frac{g_j^o}{\overline{R}T} + \ln(\sigma_j) - \ln(\sigma_m) + \ln(\frac{p}{p^o}) - \sum_{i=0}^{i=\overline{n_a}} \pi_i \eta_{ij} \qquad j = 0 \rightarrow \overline{n_s}$$

Now when taking the derivative of the above with respect to $\ln(\sigma_k)$, one notices that all the terms are constant except for the $\ln(\sigma_j)$ terms, and this too is only a variable if $k = j$. Therefore the first derivative in Eq. 15 can be evaluated as,

$$\sum_{k=0}^{k=\overline{n_s}} \frac{\partial f_j}{\partial \ln(\sigma_k)} = \delta_{jk} \qquad j = 0 \rightarrow \overline{n_s} \tag{16}$$

Again, for the second derivative term in Eq. 15 all the terms in f_j are constant but for $\ln(\sigma_m)$ thus,

$$\frac{\partial f_j}{\partial \ln(\sigma_m)} = -1 \qquad j = 0 \rightarrow \overline{n_s} \tag{17}$$

In order to evaluate the last derivative term from Eq. 15, one can make use of the following relation from the Calculus,

$$\frac{\partial y}{\partial z} = \frac{\partial y}{\partial x}\frac{\partial x}{\partial z} \tag{18}$$

which when applied to the particular case here yields,

$$\frac{\partial f_s}{\partial \ln(T)} = T\frac{\partial f_s}{\partial T} \tag{19}$$

Now since both π_i and η_{ij} are constants, the final derivative of f_j with respect to temperature (or more exactly $\ln(T)$) can be reduced to (applying the result of Eq. 19),

$$\frac{\partial f_j}{\partial \ln(T)} = -\frac{h_j}{\overline{R}T} \qquad j = 0 \rightarrow \overline{n_s} \tag{20}$$

Therefore, combining the results of Eqs. 16, 17, and 20 with Eq. 15 and remembering that these results apply over all the species one obtains (rearranging and re-substituting k for j while removing the Kronecker delta),

$$\boxed{\Delta \ln(\sigma_k) = \Delta \ln(\sigma_m) + \frac{h_k}{\overline{R}T}\Delta \ln(T) - \frac{g_k}{\overline{R}T} + \sum_{i=0}^{i=\overline{n_a}} \pi_i \eta_{ik} \qquad k = 0 \rightarrow \overline{n_s}} \tag{21}$$

With this equation, if one can solve for $\Delta \ln(\sigma_m)$, $\Delta \ln(T)$, and π_i (of which there are n_a of the latter variable) then one can use this result to obtain the equilibrium molar amounts of each species being considered in the combustion process. To solve for these variables, the remaining functional equations derived earlier can be used.

Using Eq. 10, taking its derivatives and substituting the results into Eq. 15 yields,

$$\sum_{k=0}^{k=\overline{n_s}} \sigma_k \eta_{ik} \Delta \ln(\sigma_k) = -\sum_{k=0}^{k=\overline{n_s}} \eta_{ik}\sigma_k + b_i^* \qquad i = 0 \rightarrow \overline{n_a}$$

Replacing $\Delta \ln(\sigma_k)$ by using Eq. 21 in the above and rearranging yields,

$$\boxed{\begin{array}{l}\sum_{j=0}^{j=\overline{n_a}}\left\{\sum_{k=0}^{k=\overline{n_s}}\sigma_k\eta_{ik}\eta_{jk}\right\}\pi_j+\left\{\sum_{k=0}^{k=\overline{n_s}}\sigma_k\eta_{ik}\right\}\Delta\ln(\sigma_m)\\ \qquad+\left\{\sum_{k=0}^{k=\overline{n_s}}\sigma_k\eta_{ik}\frac{h_k}{\overline{RT}}\right\}\Delta\ln(T)\end{array}=b_i^*-\sum_{k=0}^{k=\overline{n_s}}\sigma_k\eta_{ik}+\sum_{k=0}^{k=\overline{n_s}}\sigma_k\eta_{ik}\frac{g_k}{\overline{RT}}} \tag{22}$$

where $i=0\rightarrow\overline{n_a}$.

Considering next the functional in Eq. 14 and repeating the derivative process yields after substitution into Eq. 15,

$$\sum_{k=0}^{k=\overline{n_s}}\sigma_k\Delta\ln(\sigma_k)-\sigma_m\Delta\ln(\sigma_m)=-\sum_{k=0}^{k=\overline{n_s}}\sigma_k-\sigma_m$$

Again replacing $\Delta\ln(\sigma_k)$ by using Eq. 21 in the above yields (after some rearranging),

$$\boxed{\begin{array}{l}\sum_{i=0}^{i=\overline{n_a}}\left\{\sum_{k=0}^{k=\overline{n_s}}\eta_{ik}\sigma_k\right\}\pi_i+\left\{\sum_{k=0}^{k=\overline{n_s}}\sigma_k-\sigma_m\right\}\Delta\ln(\sigma_m)\\ \qquad+\left\{\sum_{k=0}^{k=\overline{n_s}}\sigma_k\frac{h_k}{\overline{RT}}\right\}\Delta\ln(T)\end{array}=\sigma_m+\sum_{k=0}^{k=\overline{n_s}}\sigma_k\left(\frac{g_k}{\overline{RT}}-1\right)} \tag{23}$$

The results from the last functional (Eq. 11) can be expressed as,

$$\sum_{k=0}^{k=\overline{n_s}}\sigma_k\frac{h_k}{\overline{RT}}\Delta\ln(\sigma_k)+\sum_{k=0}^{k=\overline{n_s}}\sigma_k\frac{c_{p_k}}{\overline{R}}\Delta\ln(T)=-\sum_{k=0}^{k=\overline{n_s}}\sigma_k\frac{h_k}{\overline{RT}}+\frac{H^*}{\overline{RT}}$$

which after substituting Eq. 21 and rearranging becomes,

$$\boxed{\begin{array}{l}\sum_{i=0}^{i=\overline{n_a}}\left\{\sum_{k=0}^{k=\overline{n_s}}\sigma_k\eta_{ik}\frac{h_k}{\overline{RT}}\right\}\pi_i+\left\{\sum_{k=0}^{k=\overline{n_s}}\sigma_k\frac{h_k}{\overline{RT}}\right\}\Delta\ln(\sigma_m)\\ \qquad+\left\{\sum_{k=0}^{k=\overline{n_s}}\sigma_k\left[\frac{c_{p_k}}{\overline{R}}+\left(\frac{h_k}{\overline{RT}}\right)^2\right]\right\}\Delta\ln(T)\end{array}=\frac{H^*}{\overline{RT}}+\sum_{k=0}^{k=\overline{n_s}}\sigma_k\frac{h_k}{\overline{RT}}\left(\frac{g_k}{\overline{RT}}-1\right)} \tag{24}$$

Using Eqs. 22, 23, and 24 one now has n_a+2 number of equations using only n_a+2 number of distinct variables ($\pi_1\ldots\pi_{n_a}$, $\Delta\ln(\sigma_m)$, and $\Delta\ln(T)$). Furthermore, these equations form a system of linear equations which can be readily solved using Gaussian elimination. If written in the form $Ax=R$ where A is the coefficient matrix, x is the solution vector, and R is a column vector of known quantities then the system looks like,

$$A=\begin{bmatrix}\sum_{k=0}^{k=\overline{n_s}}\eta_{0k}\eta_{0k}\sigma_k & \cdots & \sum_{k=0}^{k=\overline{n_s}}\eta_{0k}\eta_{\overline{n_a}k}\sigma_k & \sum_{k=0}^{k=\overline{n_s}}\eta_{0k}\sigma_k & \sum_{k=0}^{k=\overline{n_s}}\eta_{0k}\sigma_k\frac{h_k}{\overline{RT}}\\ \vdots & \ddots & \vdots & \vdots & \vdots\\ \sum_{k=0}^{k=\overline{n_s}}\eta_{\overline{n_a}k}\eta_{0k}\sigma_k & \cdots & \sum_{k=0}^{k=\overline{n_s}}\eta_{\overline{n_a}k}\eta_{\overline{n_a}k}\sigma_k & \sum_{k=0}^{k=\overline{n_s}}\eta_{\overline{n_a}k}\sigma_k & \sum_{k=0}^{k=\overline{n_s}}\eta_{\overline{n_a}k}\sigma_k\frac{h_k}{\overline{RT}}\\ \sum_{k=0}^{k=\overline{n_s}}\eta_{0k}\sigma_k & \cdots & \sum_{k=0}^{k=\overline{n_s}}\eta_{\overline{n_a}k}\sigma_k & \sum_{k=0}^{k=\overline{n_s}}\sigma_k-\sigma_m & \sum_{k=0}^{k=\overline{n_s}}\sigma_k\frac{h_k}{\overline{RT}}\\ \sum_{k=0}^{k=\overline{n_s}}\eta_{0k}\sigma_k\frac{h_k}{\overline{RT}} & \cdots & \sum_{k=0}^{k=\overline{n_s}}\eta_{\overline{n_a}k}\sigma_k\frac{h_k}{\overline{RT}} & \sum_{k=0}^{k=\overline{n_s}}\sigma_k\frac{h_k}{\overline{RT}} & \sum_{k=0}^{k=\overline{n_s}}\sigma_k\left[\frac{c_{p_k}}{\overline{R}}+\left(\frac{h_k}{\overline{RT}}\right)^2\right]\end{bmatrix} \tag{25}$$

with

$$x = \begin{bmatrix} \pi_1 \\ \vdots \\ \pi_{n_a} \\ \Delta \ln(\sigma_m) \\ \Delta \ln(T) \end{bmatrix} \qquad R = \begin{bmatrix} b_0^* + \sum_{k=0}^{k=\overline{n_s}} \eta_{0k} \sigma_k (\frac{g_k}{RT} - 1) \\ \vdots \\ b_{\overline{n_a}}^* + \sum_{k=0}^{k=\overline{n_s}} \eta_{\overline{n_a}k} \sigma_k (\frac{g_k}{RT} - 1) \\ \sigma_m + \sum_{k=0}^{k=\overline{n_s}} \sigma_k (\frac{g_k}{RT} - 1) \\ \frac{H^*}{RT} + \sum_{k=0}^{k=\overline{n_s}} \sigma_k \frac{h_k}{RT} (\frac{g_k}{RT} - 1) \end{bmatrix} \tag{26}$$

The actual change in kmols of each species can be found using the solution vector x and Eq. 21.

2.2 Numerical Solution

The numerical solution of the Gibbs Minimization Technique involves the solution of the system of equations described by Eqs. 25 and 26. However, depending on the initial values of the amounts of kmols of each species and the initial equilibrium temperature (which are in essence simply a guess at the equilibrium solution), the final answer is obtained only after several inversions of the matrix in Eq. 25 (one must be careful to distinguish between the initial conditions for combustion [i.e. total temperature and fuel to oxidizer ratio, which do not change and are used for calculating properties such as H^* and b_i^*] and the initial guess at the equilibrium solution [i.e. the initial values of σ_k and T]). In order to ensure that the numerical process remains stable, a relaxation parameter is used which ensures that the rates of change do not rise so fast as to lead to numerical instability of the iterative process. As the process approaches the equilibrium solution, the relaxation parameter goes to 1 in essence removing any damping near the final answer.

The relaxation parameter is calculated as follows. For species whose kmol amounts are greater than some threshold value (the limit below which a species is considered minor, eg. $1x10^{-8}$ kmols) and whose $\Delta \ln(\sigma_k)$ is positive one calculates a variable β_1,

$$\beta_1 = \frac{2}{\max\left(|\Delta \ln(T)|, |\Delta \ln(\sigma_m)|, |\Delta \ln(\sigma_k)|\right)} \tag{27}$$

while for the remaining species (those below the threshold value, the minor species) with positive $\Delta \ln(\sigma_k)$ values one calculates β_2 as

$$\beta_2 = \frac{\ln(1x10^{-4}) - \ln(\sigma_k) + \ln(\sigma_m)}{\Delta \ln(\sigma_k) - \Delta \ln(\sigma_m)} \tag{28}$$

with these two values found, one then calculates the final relaxation parameter, β, as the minimum of these two values and 1,

$$\beta = \min(1, \beta_1, \beta_2) \tag{29}$$

With the relaxation parameter calculated one can find new values of the desired variables using the relations,

$$\ln(T_{new}) = \ln(T_{old}) + \beta \Delta \ln(T)$$

$$\ln(\sigma_{m_{new}}) = \ln(\sigma_{m_{old}}) + \beta \Delta \ln(\sigma_m)$$

$$\ln(\sigma_{k_{new}}) = \ln(\sigma_{k_{old}}) + \beta \Delta \ln(\sigma_k) \qquad k = 0 \rightarrow \overline{n_s}$$

The equilibrium solution is obtained when some suitably defined convergence tolerance is met, such as

$$\frac{|\sum_{k=0}^{k=\overline{n_s}} \sigma_k - \sigma_m|}{\sigma_m} < 1x10^{-7} \tag{30}$$

The last point to note in solving this system is the selection of initial conditions. It has been found that the following initial conditions work very well, leading to a converged solution for most cases in under approximately 30 iterations,

TABLE 2.
Suggested Initial Conditions

σ_m [kmol]	σ_k [kmol]	T_{eq} [K]
0.1	$0.1/n_s^*$	3800

* where n_s is the total number of species under consideration

3 Axisymmetric Nozzle Design Theory

For the nozzle design methodology, the inviscid flow of a perfect gas (γ = constant) will be assumed throughout the derivation (a viscous correction being applied after an inviscid contour is determined). It will also be assumed that the final nozzle design will produce radial flow over a given region downstream of the sonic point, allowing certain pertinent radial flow equations to be used when determining nozzle properties. The remaining portions of the nozzle will then be determined based on the existing radial flow region. In this fashion, the desired Mach number distribution along the nozzle centreline will be determined, and a nozzle shape will be found which produces this set distribution. Also, the expansion process through the nozzle will be assumed to occur without chemical reactions (i.e. frozen flow) thereby keeping the mixture composition constant from the combustion chamber to the nozzle exit.

The various flow zones within the diverging portion of the nozzle are shown in Fig. 1. The radial flow portion of the nozzle is bounded by the points B and D, and thus all radial flow equations apply only within this region. The distance ϵ is the distance downstream of the geometric throat at which the flow along the axisymmetric axis is sonic (note that for real nozzles the sonic line is not straight but slightly curved, shown in the figure as the line extending from the throat roof to point A). Point O is the origin of the radial flow region, which does not necessarily co-incide with the geometric throat, and point F is the distance at which the flow has reached the design exit Mach number (note that here, the angle of the characteristic originating from point F is simply $\sin^{-1}(\frac{1}{M_F})$). Point C is the location of the maximum expansion angle, which is also an inflection point since the nozzle is restricted from increasing in curvature past this point.

3.1 Inviscid Nozzle Design

$$\boldsymbol{q} \cdot \nabla(\frac{q^2}{2}) - a^2(\nabla \cdot \boldsymbol{q}) = 0 \tag{31}$$

The *gas dynamic equation* as shown above can be used as the starting point for developing the properties of a radial flow region (noting that $\boldsymbol{q}$ is the velocity vector, q is the magnitude of the velocity vector, and a is the speed of sound). In spherical co-ordinates (which are the most convenient to use when considering a radial flow, since the flow travels outwards in all directions from a single source) the gradient of a vector can be expressed as,

$$\nabla \cdot \boldsymbol{q} = \frac{1}{r^2}\frac{\partial}{\partial r}(r^2 q_r) + \frac{1}{r\sin\theta}\frac{\partial}{\partial \theta}(q_\theta \sin\theta) + \frac{1}{r\sin\theta}\frac{\partial q_\phi}{\partial \phi} \tag{32}$$

Applying the radial flow condition requires that the velocity in both angular directions be zero (i.e. $q_\theta = q_\phi = 0$) thus reducing the above operator to,

$$\nabla \cdot \boldsymbol{q} = \frac{1}{r^2}\frac{d}{dr}(r^2 q_r) = \frac{dq}{dr} + 2\frac{q}{r} \tag{33}$$

where $q_r = q$ since there is only velocity in one co-ordinate direction.
The ∇ operator on a scalar quantity in spherical co-ordinates can be written as,

$$\nabla q = \frac{\partial q}{\partial r} + \frac{1}{r}\frac{\partial q}{\partial \theta} + \frac{1}{\sin\theta}\frac{\partial q}{\partial \phi} \tag{34}$$

which after applying the radial flow constraints reduces to,

$$\nabla q = \frac{dq}{dr} \tag{35}$$

Applying the results of Eqs. 33 and 35 to Eq. 31 (and noting that $\boldsymbol{q} = q_r = q$ for radial flow) yields,

$$\boxed{(1 - M^2)\frac{dq}{dr} - 2\frac{q}{r} = 0} \tag{36}$$

This equation is the governing equation for inviscid radial flow.

3.1.1 Radial Flow Region

Starting with the fundamental radial flow equation derived in Eq. 36 one can determine the relation between the Mach number at a given location and the distance of this point from the radial flow source. This is a key relationship given that it is the Mach number distribution along the nozzle centreline (which is simply the radius along a particular ray from the radial flow source) that will be used to dictate the final nozzle contour. The equations developed in this section apply between points B and D in Fig. 1

Starting by defining a non-dimensional velocity as,

$$\boxed{W = \frac{q}{a^*}} \tag{37}$$

where a^* is the critical speed of sound (at M = 1), this non-dimensional velocity can be related to the Mach number as follows. Since $Ma = q$ and $Wa^* = q$ one can write,

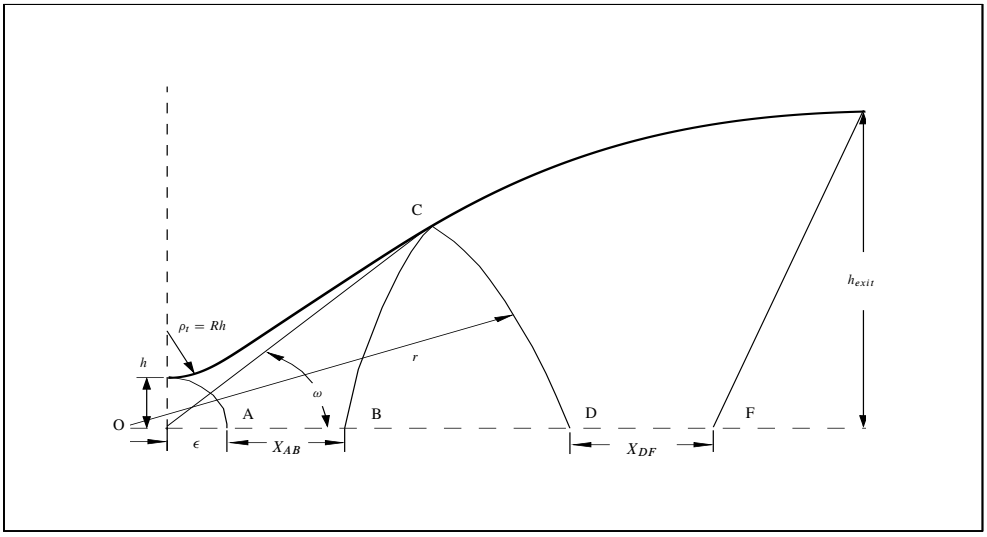

FIGURE 1. Nomenclature for Nozzle Design

$$(\frac{M}{W})^2 = (\frac{a^*}{a})^2$$

while from isentropic relations one can express the ratio of sound speeds as,

$$(\frac{a^*}{a})^2 = \frac{2}{(\gamma+1)}\Big\{1 + \frac{\gamma-1}{2}M^2\Big\} \tag{38}$$

thus one can write,

$$(\gamma+1)M^2 = W^2\Big\{2 + (\gamma-1)M^2\Big\}$$

After isolating for W^2 and dividing through by $(\gamma-1)$, while defining k as,

$$\boxed{k = \tfrac{\gamma+1}{\gamma-1}} \tag{39}$$

one can rewrite the above expression as,

$$\boxed{W^2 = \tfrac{kM^2}{k-1+M^2}} \tag{40}$$

Isolating M^2 in Eq. 40 yields an expression for the Mach number from the non-dimensional velocity,

$$\boxed{M^2 = \tfrac{W^2(k-1)}{k-W^2}} \tag{41}$$

Going back to the governing equation for radial flow (Eq. 36) and rearranging slightly,

$$\frac{M^2-1}{2q}dq = \frac{1}{r}dr$$

one can use the definition of the non-dimensional velocity (Eq. 37) from which one can write $dq = a^* dW$ and when combined with Eq. 41 allows the above relation to be expressed completely in terms of W. Integrating the resulting expression from the sonic point (at which point $r = r_{cr}$ and $W = M = 1$) to some general point r one obtains,

$$\int_{r_{cr}}^{r}\frac{1}{r}dr = \frac{1}{2}\Big\{\int_{W=1}^{W}\frac{M^2}{W}dW - \int_{W=1}^{W}\frac{1}{W}dW\Big\} \tag{42}$$

Equation 42 can be integrated analytically if one assumes a perfect gas (hence k is a constant with respect to the variable of integration W) by letting $x = W^2$ (and thus $\frac{1}{2}dx = WdW$),

$$\ln(\frac{r}{r_{cr}}) = \frac{1}{2}\Big\{(k-1)\frac{1}{2}\int_{W=1}^{W}\frac{1}{k-x}dx - \ln(W)|_{W=1}^{W}\Big\}$$

Re-substituting back for W and applying the limits yields,

$$\ln(\frac{r}{r_{cr}}) = \ln\Big\{\frac{(k-W^2)^{\frac{1}{4}(1-k)}}{W^{\frac{1}{2}}(k-1)^{\frac{1}{4}(1-k)}}\Big\}$$

taking the exponential of both sides and defining a non-dimensional radius, $\overline{r}$, as,

$$\boxed{\overline{r} = \tfrac{r}{r_{cr}}} \tag{43}$$

yields,

$$\overline{r} = \frac{(k-1)^{\frac{1}{4}(k-1)}}{W^{\frac{1}{2}}(k-W^2)^{\frac{1}{4}(k-1)}}$$

to phrase this result in a more usable form one can square both sides while multiplying the right side by W_k/W_k, substituting for M using Eq. 41, and rearranging to get,

$$\overline{r}^2 = \frac{M^k}{W^k}\frac{1}{M} = (\frac{M^2}{W^2})^{\frac{k}{2}}\frac{1}{M}$$

But from Eq. 40 one can express W in terms of M to yield,

$$\boxed{\overline{r}^2 = \frac{1}{M}\left\{\frac{k-1+M^2}{k}\right\}^{\frac{k}{2}}} \tag{44}$$

Equation 44 now gives us a means of determining the Mach number vs. non-dimensional radius within the radial flow region of the nozzle. Another key quantity in the radial flow region is the integrated angle, θ, which for radial flows can be shown to be equal to half the Prandtl-Meyer expansion angle for 2D flows. This angle represents the angle through which a supersonic flow must be turned in order to be accelerated from a Mach number of 1 to the given Mach number M, and can be expressed for a perfect gas as,

$$\boxed{\theta = \frac{1}{2}\left\{k^{\frac{1}{2}}\tan^{-1}\left[\frac{M^2-1}{k}\right]^{\frac{1}{2}} - \tan^{-1}(M^2-1)^{\frac{1}{2}}\right\}} \tag{45}$$

This angle can be used to help determine the boundaries of the radial flow region, as although Eq. 44 will yield a radial position for a given Mach number, the Mach number at points D, C, and B are all unknown. However, from the geometry of the nozzle itself, it can be seen that the difference between the integrated angles at points D and C must be equal to the physical angle COD in Fig. 1 which is the set maximum expansion angle ω. Therefore, if the Mach number at point D is known, then so is the integrated angle at this point. With this one can then fully determine point C using the maximum expansion angle and Eq. 45 to get the Mach number at C, then Eq. 44 to get the radial position of this point from the previously determined M_C. The same procedure can be used to find point B only in this case the difference between the integrated angles at points D and B is equal to twice the maximum expansion angle. Thus, using Eqs. 44 and 45 one can fully determine the Mach number distribution within the radial flow region provided the Mach number at point D is known.

3.1.2 Final Expansion Region

From the previous section, all that is required to fully describe the radial flow region is the Mach number at the end of this region, M_D. However, from the set nozzle parameters only the Mach number at point F is known since at this point the flow has been accelerated to the exit Mach number. Let the Mach number distribution between points D and F be described by a fifth order polynomial of the form,

$$W = D_0 + D_1\xi + D_2\xi^2 + D_3\xi^3 + D_4\xi^4 + D_5\xi^5 \tag{46}$$

where along the axisymmetric axis,

$$\xi = \frac{\overline{r} - \overline{r}_D}{\overline{X}_{DF}}$$

It should be noted that all the non-dimensional quantities above are non-dimensionalized by the critical radius, as was done in Eq. 43. In order to determine the co-efficients D_0 through D_5 one must make use of six boundary conditions. Therefore, specifying the velocity and its derivatives up to second order at each of the boundaries gives,

where it is noted that,

$$\frac{dW}{d\xi} = D_1 + 2D_2\xi + 3D_3\xi^2 + 4D_4\xi^3 + 5D_5\xi^4 \tag{47}$$

$$\frac{d^2W}{d\xi^2} = 2D_2 + 6D_3\xi + 12D_4\xi^2 + 20D_5\xi^3 \tag{48}$$

TABLE 3.
Non-Dimensional Boundary Conditions

Point	ξ	Velocity (W)	Acceleration (W')	Impulse (W'')
D	0	W_D	$(\frac{dW}{d\overline{r}})_D = W'_D$	$(\frac{d^2W}{d\overline{r}^2})_D = W''_D$
F	1	W_F	0	0

At point D, since $\xi = 0$, applying the first boundary condition yields a direct solution for D_0,

$$\boxed{D_0 = W(0) = W_D} \tag{49}$$

and similarly when applying the acceleration condition at point D one obtains D_1 (while noting that $d\xi X_{DF} = d\overline{r}$),

$$\boxed{D_1 = \frac{dW(0)}{d\xi} = \overline{X}_{DF}\frac{dW(0)}{d\overline{r}} = \overline{X}_{DF}W'_D} \tag{50}$$

Applying the last boundary condition at point D yields,

$$\boxed{D_2 = \tfrac{1}{2}\overline{X}^2_{DF}W''_D} \tag{51}$$

Moving on to point F, skipping the velocity boundary condition for the moment and applying the acceleration condition yields,

$$D_4 = -\frac{1}{4}(D_1 + 2D_2 + 3D_3 + 5D_5)$$

Using the impulse condition at point F yields for D_5,

$$D_5 = -\frac{1}{20}(2D_2 + 6D_3 + 12D_4)$$

which after using the previous result for D_4 gives,

$$D_5 = \frac{1}{5}(3D_1 + 4D_2 + 3D_3)$$

Now using the velocity condition at F and isolating D_3 yields,

$$D_3 = W_F - D_0 - D_1 - D_2 - D_4 - D_5$$

which when the results for D_0, D_4, and D_5 are substituted results in,

$$\boxed{D_3 = 10(W_F - W_D) - 6D_1 - 3D_2} \tag{52}$$

Going back and replacing D_3 in the expressions for D_4 and D_5 yields,

$$\boxed{D_4 = -15(W_F - W_D) + 8D_1 + 3D_2} \tag{53}$$

$$\boxed{D_5 = 6(W_F - W_D) - 3D_1 - D_2} \tag{54}$$

At this point, it is noted that there are four apparent unknowns in the various co-efficients, W_D, W'_D, W''_D, and $\overline{X}_{DF}$. In order to ensure a smooth increase in velocity along the axisymmetric axis between points D and F, it can be assumed that $D_5 = 0$ which then allows for the solution of $\overline{X}_{DF}$ from Eq. 54 as,

$$\overline{X}_{DF} = -\frac{3W'_D}{W''_D}\left\{1 - \sqrt{1 + \frac{4W''_D(W_F - W_D)}{3W'^2_D}}\right\} \tag{55}$$

At this point we have reduced the number of unknowns to three, since the non-dimensional length $\overline{X}_{DF}$ is now a function of W_D, W'_D, and W''_D. Since point D is part of the radial flow region, the analytical expressions developed for this type of flow can be used here as well. Going back to Eq. 44 and using the relation expressed in Eq. 41 one can obtain an equation for $\overline{r}^2$ in terms of W,

$$\boxed{\overline{r}^2 = \frac{1}{W}\left\{\frac{(k-1)}{(k-W^2)}\right\}^{\frac{(k-1)}{2}}} \tag{56}$$

Taking the natural logarithm of both sides and differentiating yields an expression for the first derivative of non-dimensional velocity with respect to the non-dimensional radius,

$$\frac{dW}{d\overline{r}} = \frac{2W(k-W^2)}{k(W^2-1)\overline{r}} = W' \tag{57}$$

The second derivative can also be found from Eq. 57 and be shown to be equal to,

$$\frac{d^2W}{d\overline{r}^2} = \frac{-W'^2[3k-6W^2+(k+2)W^4]}{2W(k-W^2)(W^2-1)} = W''^2 \tag{58}$$

With Eqs. 57 and 58 one can find the values of W'_D and W''_D from the value of W_D alone, thus reducing the number of unknowns involved in determining the desired polynomial co-efficients to one, namely W_D. This was also the sole unknown required for the complete determination of the radial flow region. To determine this value, one can again make use of Eq. 55 by noting that the value under the root must be positive to ensure a real solution. Therefore,

$$(W_F - W_D) \geq -\frac{3}{4}\frac{W'^2_D}{W''_D} \tag{59}$$

With this, one has a guide to selecting W_D, but the actual value must be chosen by the designer. As a good first guess, $W_F - W_D$ can be taken as 1.5% of W_F and increased until the criteria in Eq. 59 is satisfied. Once $W_F - W_D$ is determined, W_D can be used to completely determine the centreline Mach number distribution from the beginning of the radial flow region through to the nozzle exit inclusive.

3.1.3 Initial Expansion Region

Having already established the Mach number distribution from the beginning of the radial flow region (point B, Fig. 1) to the nozzle exit, the only region remaining to be defined is the initial expansion region near the nozzle throat (from point A to B, Fig. 1). Since the final expansion region was modeled using a fourth order polynomial (recalling that the fifth co-efficient, D_5, was assumed zero), for consistency, the initial expansion region will be treated similarly. Thus one can write for the segment along the axisymmetric axis between points A and B,

$$W = C_0 + C_1\eta + C_2\eta^2 + C_3\eta^3 + C_4\eta^4 \tag{60}$$

where along the axis,

$$\eta = \frac{\overline{r} - \overline{r}_A}{\overline{X}_{AB}}$$

As for the final expansion region, all the non-dimensional lengths are divided by the critical radius (see Eq. 43). In order to determine the co-efficients C_0 through C_4 one again has the option of applying six boundary conditions. Specifying the velocity and its derivatives up to second order at each of the boundaries requires the derivatives of Eq. 60 up to second order while the boundary conditions themselves are,

Since the radial flow region includes point B, the non-dimensional velocity and position at point B (W_B and $\overline{r}_B$ respectively) are known quantities. As well, Eqs. 57 and 58 can both be used to determine W'_B and W''_B making the boundary conditions at the end of the initial expansion region completely known. However, at the beginning of this region the flow has just reached sonic speed, thus the nozzle throat region near point A is an area of transonic flow.

TABLE 4. Non-Dimensional Boundary Conditions

Point	η	Velocity (W)	Acceleration (W')	Impulse (W'')
A	0	1	$(\frac{dW}{d\overline{r}})_A = W'_A$	$(\frac{d^2W}{d\overline{r}^2})_A = W''_A$
B	1	W_B	$(\frac{dW}{d\overline{r}})_B = W'_B$	$(\frac{d^2W}{d\overline{r}^2})_B = W''_B$

This requires a specialized technique to solve, since one dimensional theory predicts a straight sonic line at the exact geometric throat of the nozzle, whereas in real applications this line is curved with the sonic point lying a finite distance downstream of the geometric throat (labeled ϵ in Fig. 1) along the axisymmetric axis (Note: this line also *starts* a finite distance upstream of the throat, but this region need not be considered in the present analysis). There are several methods available to describe this transonic region (Sauer's Method, Hall's Method, Kliegel's Method) however Kliegel's Method (which is a modified version of Hall's Method) will be used here.

In Kliegel's analysis the non-dimensional velocity distribution along the axisymmetric axis in the throat region is given in the form of an equation in terms of S (where $S = R + 1$). In obtaining this solution, the throat region is assumed to be a circular arc of radius (ρ_t) while the parameter R is the ratio of this radius to the half height, or radius, of the nozzle throat (h) thereby creating the relation $Rh = \rho_t$. With the velocity distribution in this form one can obtain its derivatives for use in application to the boundary conditions, where at point A,

$$(\frac{dW}{d\overline{r}})_A = \lambda R_1 \Big\{1 - \frac{4\gamma - 3}{24S} + \frac{652\gamma^2 + 15\gamma + 333}{6912S^2}\Big\} \tag{61}$$

$$(\frac{d^2W}{d\overline{r}^2})_A = (\lambda R_1)^2 \Big\{1 - \frac{2\gamma}{3} + \frac{4\gamma^2 + 69\gamma + 15}{96S}\Big\} \tag{62}$$

$$(\frac{d^3W}{d\overline{r}^3})_A = (\lambda R_1)^3 \Big\{\frac{4\gamma^2 - 57\gamma + 27}{24}\Big\} \tag{63}$$

where $\lambda = \sqrt{\frac{2}{(\gamma+1)S}}$ and $R_1 = \frac{r_{cr}}{h}$. As well as yielding these derivatives Kliegel's analysis also yields the sonic point's distance downstream of the geometric nozzle throat (ϵ) as,

$$\overline{\epsilon} = \frac{\epsilon}{r_{cr}} = \frac{1}{4\lambda S}\Big\{1 - \frac{4\gamma - 15}{72S} + \frac{412\gamma^2 + 270\gamma + 909}{10368S^2}\Big\} \tag{64}$$

Therefore, if S is known (which requires R to be known) then the location of point A can be determined from Eq. 64. However, the nozzle upper wall arc radius in the throat region, ρ_t, cannot simply be assigned a value like a design variable, but must be calculated based on further restrictions to be derived.

In a manner similar to that in the final expansion region, the boundary conditions can be applied to Eq. 60 to obtain the various co-efficients C_O through C_4. Starting with the boundary conditions at point A, through direct substitution (and noting that $d\eta X_{AB} = d\overline{r}$),

$$\boxed{C_0 = 1} \tag{65}$$

$$\boxed{C_1 = \overline{X}_{AB} W'_A} \tag{66}$$

$$\boxed{C_2 = \tfrac{1}{2}\overline{X}^2_{AB} W''_A} \tag{67}$$

Considering next the boundary conditions at point B, the velocity condition yields (while substituting for C_0),

$$C_3 = (W_B - 1) - C_1 - C_2 - C_4$$

while the acceleration condition gives,

$$C_3 = \frac{1}{3}(\overline{X}_{AB} W'_B - C_1 - 2C_2 - 4C_4)$$

Combining these two results yields for C_4,

$$\boxed{C_4 = -3(W_B - 1) + W'_B \overline{X}_{AB} + 2C_1 + C_2} \tag{68}$$

and from back substitution one can get C_3 as,

$$\boxed{C_3 = 4(W_B - 1) - W'_B \overline{X}_{AB} - 3C_1 - 2C_2} \tag{69}$$

At this point, one still has three unknowns, W'_A, W''_A and $\overline{X}_{AB}$, in that although Eqs. 61 and 62 can be used to find W'_A and W''_A, the values of both S and R_1 are needed to use these equations. Therefore, applying the remaining boundary condition at point B yields,

$$\frac{d^2W(1)}{d\eta^2} = \overline{X}^2_{AB} \frac{d^2W(1)}{d\overline{r}^2} = \overline{X}^2_{AB} W''_B = 2C_2 + 6C_3 + 12C_4$$

Using Eqs. 67, 69 and 68 to replace C_2, C_3, and C_4 respectively yields a quadratic expression for $\overline{X}_{AB}$,

$$(W''_A - W''_B)\overline{X}^2_{AB} + 6(W'_A + W'_B)\overline{X}_{AB} - 12(W_B - 1) \tag{70}$$

This reduces $\overline{X}_{AB}$ to a function of both remaining unknowns, but one is still left with finding values for S and R_1. However, in applying Kliegel's Method it is suggested that the second derivative of the nozzle contour in the region approximately one diameter downstream of the geometric throat approximate the shape of a circle or hyperbola. This criteria is best satisfied if the co-efficient C_3 is held equal to the value $\frac{1}{6}W'''_A \overline{X}^3_{AB}$,

$$C_3 = \frac{1}{6}W'''_A \overline{X}^3_{AB} = 4(W_B - 1) - W'_B \overline{X}_{AB} - 3C_1 - 2C_2$$

which after using Eqs. 66 and 67 in the above yields,

$$W'''_A \overline{X}^3_{AB} + 6W''_A \overline{X}^2_{AB} + 6(W'_B + 3W'_A)\overline{X}_{AB} - 24(W_B - 1) = 0 \tag{71}$$

Unfortunately this does not completely define the problem, as the determination of the derivatives at point A is still problematic in that the variables S and R_1 are not completely independent (as will be shown, R_1 depends on S). However, Eqs. 70 and 71 can be used as a means of checking the accuracy of the values for S and R_1 given that once $\overline{X}_{AB}$ is found using a particular set of S and R_1 values, one can then substitute this value and the corresponding derivative values into Eq. 71 to check the result. If Eq. 71 is satisfied, a solution has been obtained.

Therefore, in order to determine the variables S and R_1 (for use in finding the derivative values at point A) one can make use of the parameter K^2, which is the ratio of the actual massflow passing through the nozzle throat (with a curved sonic line) to the massflow passing through the nozzle assuming a straight sonic line (one dimensional flow). From Kliegel's Method this value can be expressed as,

$$K^2 = 1 - \frac{\gamma - 1}{96S^2}\left\{1 - \frac{8\gamma - 27}{24S} + \frac{754\gamma^2 - 757\gamma + 3615}{2880S^2}\right\} \tag{72}$$

while the ratio of critical radius to throat radius, R_1, can be expressed

$$R_1 = \frac{r_{cr}}{h} = \frac{1}{2}K \csc(\frac{\omega}{2}) \tag{73}$$

Equations 72 and 73 provide the link between S and R_1. Similar to the final expansion region however, one is now forced to guess at a value for one of the required variables and then iterate slowly until all the criteria are met. In this case, one must first guess at a value of S (or

R since $S = R + 1$). With this, one can get a value for R_1 from Eqs. 72 and 73 and with these values one can then use Eqs. 61, 62, and 63 to get W_A', W_A'', and W_A''' which in turn can be used in Eq. 70 to find a value for $\overline{X}_{AB}$. This value is then checked using Eq. 71 and if this equation is not satisfied then the value of S can be changed until the convergence criteria is met. Once $\overline{X}_{AB}$, W_A', and W_A'' are determined, the co-efficients C_0 through C_4 can be found thereby completely determining the Mach number distribution along the axisymmetric axis in the initial expansion region.

As a final note, since the nozzle contour is determined only at points along the characteristic mesh, the final velocity along the wall at the precise throat location cannot be determined using the method of characteristics since the point closest to the nozzle throat along the prescribed Mach number distribution is located a finite distance *downstream* of the geometric throat. Therefore, making use of Kliegel's analysis once again, the throat wall velocity can be expressed as,

$$W_{throat} = 1 + \frac{1}{4S} - \frac{14\gamma - 57}{288S^2} + \frac{2364\gamma^2 - 3915\gamma + 14337}{82944S^3} \tag{74}$$

3.1.4 Nozzle Wall Determination

With the desired Mach number distribution established and the final Mach line originating from point F, one has everything required to use the two-dimensional method of characteristics to determine the flowfield within the diverging section of the nozzle. However, what is still lacking is a means of knowing when to stop marching the characteristics in the direction perpendicular to the nozzle axis. This is of critical importance as this stopping point determines the upper wall of the nozzle, which is the desired quantity. Therefore, going back to the radial flow region, one can make use of the stream function, ψ, and determine its value at the nozzle boundary.

Since the difference between stream functions at any two points within a flow is equal to the mass flow between the streamlines on which the stream functions are taken, if one knows the stream function value on the nozzle axis, plus the value at *ANY* point on the nozzle wall, then this difference must be constant given that the the mass flow through the nozzle is constant (or from another viewpoint, since the flow must follow the contour of the nozzle wall, the wall itself is a streamline. Knowing the value of the stream function at a single point along a streamline yields the value along all points of the streamline, thus finding the nozzle contour is equivalent to finding a streamline with a specific stream function value).

Using the properties of radial flow, considering an incremental area on a sphere of radius r bounded by the angles α and $\alpha + d\alpha$ one can write the differential stream function as

$$d\psi = \rho q(\pi r^2 \sin\alpha d\alpha) \tag{75}$$

Integrating Eq. 75 from the nozzle axis to some angle α,

$$\int_{\alpha=0}^{\alpha} d\psi = \rho q \pi r^2 \int_{\alpha=0}^{\alpha} \sin\alpha d\alpha = \psi = -\rho q \pi r^2 \cos\alpha|_0^{\alpha}$$

Therefore one can write,

$$\psi = \rho q \pi r^2 (1 - \cos\alpha) \tag{76}$$

where α is a physical angle between the axisymmetric axis, the origin of the radial flow zone, and some point above the axis (which is not to be confused with the integrated angle θ in Eq. 45). Non-dimensionalizing this value by the critical radius r_{cr}, the sonic sound speed a^*, the total density (found from the nozzle chamber conditions) ρ_o, and π yields,

$$\boxed{\overline{\psi} = \overline{\rho} W \overline{r}^2 (1 - \cos\alpha)} \tag{77}$$

where $\overline{\rho} = \frac{\rho}{\rho_o}$. Since point C lies within the radial flow region, Eq. 77 applies here. Further, the physical angle α at point C is known since this is also the location of the maximum expansion angle, ω. For isentropic flow the density ratio is a function of Mach number alone (and γ, but this is a property of the fluid, not the flow), which in turn is dependent only on

W within the radial flow region (see Eq. 41). Therefore, with the centreline Mach number distribution (which yields W_C and $\overline{r}_C$) one has all the information required to determine the value of the non-dimensional stream function at point C, which is a constant along the nozzle wall.

With the value of the stream function at the nozzle wall fixed, all that remains is to calculate the incremental stream function at each intersection point when applying the method of characteristics. To do this, one requires the differential of the non-dimensional stream function with respect to a change in height above the axisymmetric axis (i.e. $\frac{d\overline{\psi}}{d\overline{y}}$). When the incremental change in $\overline{y}$ is small then a good approximation for $d\overline{\psi}$ (given by Evvard) is,

$$\int_A^B d\overline{\psi} = \overline{\psi}_B - \overline{\psi}_A = \left\{ (\frac{\overline{\rho} W}{4M \sin(\mu + \theta_f)})_A + (\frac{\overline{\rho} W}{4M \sin(\mu + \theta_f)})_B \right\} (\overline{y}_B^2 - \overline{y}_A^2) \quad (78)$$

where μ is the Mach angle ($\sin^{-1}[1/M]$), θ_f here is the flow angle ($\tan^{-1}[v/u]$), and $\overline{y}$ is the perpendicular distance from the axisymmetric axis divided by the critical radius (y/r_{cr}).

In most cases, the intersection of two characteristics will not occur at the exact location of the nozzle wall (i.e. the value of the stream function will be slightly higher than the wall value at the final intersection) and hence an interpolation procedure must be used to determine the distance from the axisymmetric axis at which the stream function reaches the correct value ($\overline{\psi}_C$). The percentage of the last increment (in the direction normal to the axis) to be applied is calculated as,

$$\beta = \frac{\overline{\psi}_c - \overline{\psi}_{j-1}}{\overline{\psi}_j - \overline{\psi}_{j-1}} \quad (79)$$

where j increases as one travels away from the axis. Since $\overline{y}^2$ is proportional to $d\overline{\psi}$ (as can be seen in Eq. 78) the nozzle wall height is determined using,

$$\overline{y}_{wall}^2 = \overline{y}_{j-1}^2 + \beta(\overline{y}_j^2 - \overline{y}_{j-1}^2) \quad (80)$$

while the remaining quantities of interest at the nozzle wall are found using,

$$\overline{x}_{wall} = \overline{x}_{j-1} + \beta(\overline{x}_j - \overline{x}_{j-1})$$

$$q_{wall} = q_{j-1} + \beta(q_j - q_{j-1})$$

$$\theta_{wall} = \theta_{j-1} + \beta(\theta_j - \theta_{j-1})$$

where again, θ_j is the flow angle, *NOT* the integrated angle from Eq. 45.

3.1.5 Dimensionalizing Nozzle Wall Co-Ordinates

Having applied the two dimensional method of characteristics and determined the nozzle shape in terms of non-dimensional co-ordinates, all that remains is to calculate the physical co-ordinates. To do this one requires the value of r_{cr} which was used to non-dimensionalize all the length variables.

Considering the mass flow through the nozzle ($\dot{m}$), this quantity can be expressed as twice the value of the non-dimensional stream function at point C (i.e. $2\overline{\psi}_C$) since $\overline{\psi}_C$ is calculated for the upper portion of the axisymmetric nozzle only (from $\alpha = 0$ to ω), thus using Eq. 77

$$\dot{m} = 2\overline{\psi}_C = 2\overline{\rho}_C W_C \overline{r}_C^2 (1 - \cos\omega)$$

However, at the nozzle exit the mass flow can be expressed as,

$$\dot{m} = \rho_F u_F (\pi h_{exit}^2) \quad (81)$$

since the flow is parallel to the axis at the exit (therefore $v = 0$) and the exit area is circular. Non-dimensionalizing the above expression in the same fashion as was done for $\overline{\psi}$ (thus dividing by ρ_o, a^*, π, and r_{cr}) and equating the two expressions for $\dot{m}$ yields,

$$\boxed{\overline{h}^2_{exit} = \frac{2\overline{\psi}_C}{\overline{\rho}_F W_F}} \tag{82}$$

Assuming a one dimensional nozzle with a straight sonic line located at the geometric throat, one can express the mass flow rate through this idealized nozzle as,

$$\dot{m}_{1D} = \rho^* a^* (\pi h^2) \tag{83}$$

Recalling the analysis used in the throat region of the nozzle, Eq. 72 yields the ratio of the actual mass flow through the nozzle to the massflow of a one-dimensional nozzle. Rewriting Eq. 72 here for convenience,

$$K^2 = 1 - \frac{\gamma - 1}{96S^2}\left\{1 - \frac{8\gamma - 27}{24S} + \frac{754\gamma^2 - 757\gamma + 3615}{2880S^2}\right\}$$

one can also calculate this parameter using the ratio of Eq. 81 to Eq. 83,

$$\frac{\dot{m}}{\dot{m}_{1D}} = \frac{\rho_F u_F \pi h^2_{exit}}{\rho^* a^* \pi h^2} = \frac{\overline{\rho}_F W_F \overline{h}^2_{exit}}{\overline{\rho}^* \overline{h}^2} = K^2$$

which allows an expression for $\overline{h}^2$ to be written as,

$$\boxed{\overline{h}^2 = \frac{\overline{\rho}_F W_F \overline{h}^2_{exit}}{K^2 \overline{\rho}^*}} \tag{84}$$

Using Eq. 82 to find $\overline{h}_{exit}$ and then Eq. 84 to find $\overline{h}$, one can then find r_{cr} from the definition of $\overline{h}$,

$$\overline{h} = \frac{h}{r_{cr}} \tag{85}$$

3.2 Viscous Nozzle Design

The previous section details the procedure for designing an axisymmetric nozzle in the absence of a boundary layer. However, in practice a nozzle created using this design procedure will in fact have a turbulent boundary layer over the majority of its length. Therefore, a method is required to adjust the inviscid nozzle contour to account for the presence of the boundary layer. One such method is that of Edenfield, where experimental correlations are used to determine the mass flow deficit, or displacement thickness (δ^*), of the boundary layer which is then related to a shift (Δy) of the nozzle contour in a direction normal to the axis. Since the displacement thickness is simply the height of a region of flow (at the freestream density and velocity) that when added to the actual mass flow (including boundary layer effects, i.e., slower moving flow near the surface) would equal the theoretical massflow through the inviscid contour in the absence of a boundary layer, one can use this value to adjust the nozzle shape to maintain the inviscid mass flow value. However, since δ^* is calculated normal to the nozzle surface (which has a slope θ_{wall}) while Δy is normal to the axisymmetric axis, a small correction needs to be applied. Considering the mass flow deficit (per unit depth) calculated from the displacement thickness,

$$\Delta\dot{m} = \rho q \delta^*$$

while if the nozzle correction height is used,

$$\Delta\dot{m} = \rho u \Delta y$$

where here u is used instead of q as Δy is parallel to the velocity component v. Noting that $u = q\cos\theta_{wall}$ and making the mass flow deficit equal as calculated from either height yields,

$$\boxed{\Delta y = \frac{\delta^*}{\cos\theta_{wall}}} \tag{86}$$

If the upper wall is increased in height by an amount equal to Δy then the nozzle contour accounting for viscosity can be written as,

$$y_{viscous} = y_{inviscid} + \Delta y = y_{inviscid} + \frac{\delta^*}{\cos\theta_{wall}} \tag{87}$$

In order to calculate the displacement thickness, Edenfield suggests the relation,

$$\delta^* = \frac{21}{50}\frac{x}{Re_{ref}^{0.2775}} \tag{88}$$

where x is the physical location downstream as measured from the nozzle throat while the reference Reynolds number is defined as,

$$Re_{ref} = \frac{\rho_{ref} q_{inv} x}{\mu_{ref}} \tag{89}$$

where q_{inv} is the velocity calculated from the inviscid profile at the given x location, while ρ_{ref} and μ_{ref} are calculated at the reference temperature and the freestream pressure (which is the pressure at the x location assuming no viscosity). The reference temperature is found from the reference enthalpy, h_{ref}, defined as,

$$h_{ref} = \frac{1}{2}(h_{wall} + h_{inv}) + \frac{11}{50}(h_{aw} - h_{inv}) \tag{90}$$

where h_{wall} is the specific enthalpy calculated at the specified wall temperature, h_{aw} is the specific adiabatic wall enthalpy, and h_{inv} is the specific enthalpy calculated from the inviscid contour at the given x location,

$$h_{inv} = h_{tot} - \frac{1}{2}q_{inv}^2 \tag{91}$$

To calculate the specific adiabatic wall enthalpy Edenfield uses (for turbulent boundary layers),

$$h_{aw} = h_{inv} + \frac{9}{10}(h_{tot} - h_{inv}) \tag{92}$$

With Eqs. 87 - 92 one has all the information required to adjust the inviscid contour to account for the presence of a turbulent boundary layer. To calculate the boundary layer thickness itself, δ_{bound}, the following relations can be applied,

$$\delta_{bound} = \frac{11}{10}x\left(\frac{\frac{39}{200}M_{inv}^{\frac{3}{8}}}{Re_x^{\frac{83}{500}}}\right) \tag{93}$$

where

$$Re_x = \frac{\rho_{inv} q_{inv} x}{\mu_{inv}} \tag{94}$$

and finally,

$$y_{bound} = y_{vis} - \frac{\delta_{bound}}{\cos\theta_{wall}} \tag{95}$$

3.3 Subsonic Nozzle Contour

Although the design of the nozzle has been detailed in full from the throat to the exit, one may wish to add a subsonic portion upstream of the throat. Since uniform flow is desired at the throat, a contoured upper wall can be used to produce the desired results. One example of such an axisymmetric contour is,

$$h_{wall} = \frac{h_{throat}}{\sqrt{1 - \left\{1 - (\frac{h_{throat}}{h_{chamber}})^2\right\} \frac{(1-\frac{x^2}{l^2})^2}{1+(\frac{x^2}{3l^2})^3}}} \tag{96}$$

where l is the distance between the combustion chamber exit and the nozzle throat (which can be taken as a percentage of the length of the diverging portion of the nozzle) while x is the distance of the location under consideration as measured from the combustion chamber exit. The value of $h_{chamber}$ can be determined from the isentropic relation for areas in a converging/diverging duct (remembering that for an axisymmetric nozzle, the area is proportional to the *square* of the radius, or nozzle half height h),

$$(\frac{h_{chamber}}{h_{throat}})^2 = \frac{A}{A^*} = \frac{1}{M_{chamber}} \left\{(\frac{2}{\gamma+1})(1 + \frac{\gamma-1}{2} M^2_{chamber})\right\}^{\frac{\gamma+1}{2(\gamma-1)}} \tag{97}$$

and the assumption of a negligible velocity exiting the combustion chamber (e.g. $M_{chamber} = 0.1$).

4 Results

4.1 Kerosene/Air Combustion

The combustion of kerosene with air can be written as follows,

$$\phi C_{12}H_{24} + 18(O_2 + 3.76N_2) \longrightarrow 12H_2O + 12CO_2 + 67.68N_2 \tag{98}$$

where air is treated on a kmol basis to be composed of $21\% O_2$ and $79\% N_2$ (and the nitrogen is treated as inert during the combustion process). The fuel to air ratio on a mass basis requires a knowledge of the molecular weight of air. However, one must be careful to make a distinction between a *kmol of air* and a kmol of an individual species, since air is actually a composite species of two more basic species (oxygen and nitrogen). Thus on a kmol basis this value can be calculated as 28.8503 kg_{air}/kmol, or, since one kmol of air actually contains 4.76 kmols of primary species (i.e. 4.76 kmol/$kmol_{air}$) then molecular weight of air per *kmol of air* is actually 4.76 x 28.8503 = 137.3274 $kg_{air}/kmol_{air}$.

Therefore from Eq. 98 for every 1 kmol of fuel there are 18 kmols of air, which is actually 18 x 4.76 = 85.68 kmols, and thus the stoichiometric fuel to air ratio on a molar basis is $(\frac{f}{a})_{st}$ 1/85.68 or 0.01167. On a mass basis using the molecular weight calculated above for air of 28.8503 kg/kmol and a molecular weight for kerosene of 168.32256 kg/kmol ($C_{12}H_{24}$) one obtains $(\frac{f}{a})_{st} = 0.06809$.

Applying the Gibbs Minimization Technique and solving for the nineteen species shown in Table 5 yields the equilibrium composition shown in Fig. 2(B) (where the equivalence ratio is unity and an initial temperature and pressure of 300 K and 1.5 MPa respectively are used).

TABLE 5.
Species Map for Figure 2

0	1	2	3	4	5	6	7	8	9
H_2	O_2	H	O	OH	H_2O	HO_2	C_2H_2	C_2H_4	CO
10	11	12	13	14	15	16	17	18	
CO_2	CH_3	CH_4	H_2CO	$C_6H_{12}O$	$C_{12}H_{24}$	N	NO	N_2	

One can see from Fig. 2(A) that as the fuel to air ratio is raised from fuel lean conditions (low ϕ) to a ϕ of approximately 1, the equilibrium combustion temperature rises reaching a peak of approximately 2400 K (which assuming isentropic expansion yields a peak throat temperature of approximately 2100 K). At stoichiometric conditions, the complete combustion mass fractions of each species can be determined directly from Eq. 98 by multiplying the number of kmols of each species by its molecular weight and dividing by the total mass of either the products or reactants (as mass is conserved during the combustion process). By doing this one finds that the mass fraction of water (H_2O, species 5) is approximately 0.082 while that of carbon dioxide (CO_2, species 10) is approximately 0.200. Both of these values are far less than the stoichiometric mass fraction of nitrogen (N_2, species 18) of 0.718. Comparing these values with those shown in Fig. 2(B) one can see that the Gibbs Minimization Technique, which although based on the assumption of chemical equilibrium and not complete combustion, appears very accurate in that it matches the complete combustion solution closely. This would indicate that the complete combustion model in Eq. 98 is an accurate model of the combustion process in this case.

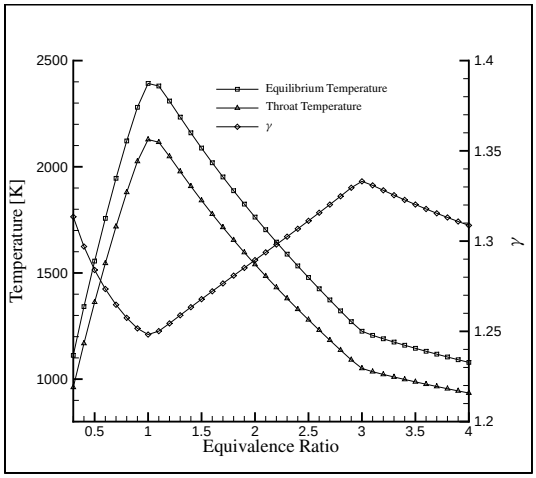

(a)

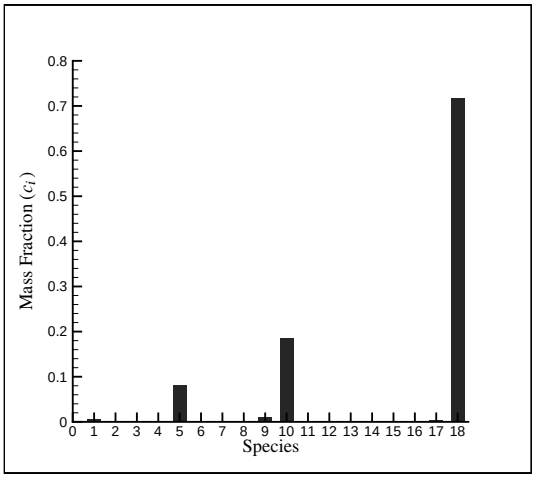

(b)

FIGURE 2. Equilibrium combustion results for (A) variable equivalence ratio and (B) equivalence ratio of 1 (stoichiometric combustion)

4.2 Kerosene/Pure Oxygen Combustion

The complete combustion reaction for the combustion of kerosene ($C_{12}H_{24}$) with pure diatomic oxygen (O_2) (which would be the case in a kerosene rocket chamber) can be written as follows,

$$\phi C_{12}H_{24} + 18O_2 \longrightarrow 12H_2O + 12CO_2 \tag{99}$$

which on a molar basis yields a fuel to air ratio, $(\frac{f}{a})_{st}$, of 1/18 or 0.05556. Using molecular weights of 168.32256 kg/kmol and 31.9988 kg/kmol for kerosene and oxygen respectively yields a $(\frac{f}{a})_{st} = 0.2916$ on a mass basis. Applying the Gibbs Minimization Technique (using sixteen species in this case as there are no species containing nitrogen) yields the equilibrium composition shown in Fig. 3(B) with initial temperature and pressure of 300 K and 1.5 MPa respectively.

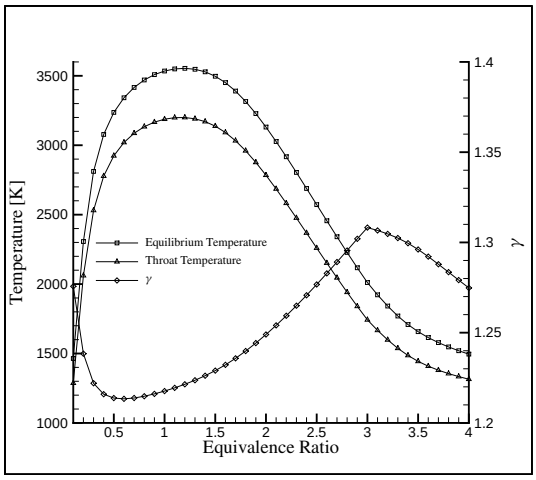

(a)

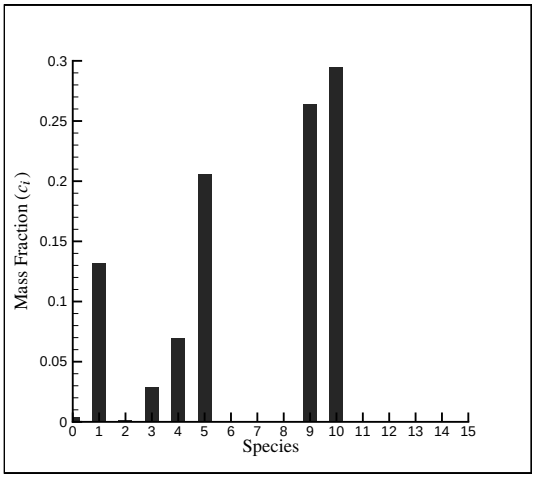

(b)

FIGURE 3. Equilibrium combustion results for (A) variable equivalence ratio and (B) equivalence ratio of 1 (stoichiometric combustion)

One of the first things to note is the significant presence of O_2 (species 1) in the post combustion mixture in Fig. 3(B). Given that the equivalence ratio in this graph is set to stoichiometric conditions ($\phi = 1$), one would expect that all the available oxidizer would be consumed by the available fuel (as was the case in the kerosene/air combustion case). However, the significant difference between the two combustion cases is the equilibrium temperature. When burned with pure O_2 as opposed to air, the resulting temperature is increased by approximately 1000 K. Around temperatures of 3500 K, many of the species involved in the combustion process start

TABLE 6.
Species Map for Figure 3 and Figure 5

0	1	2	3	4	5	6	7	8
H_2	O_2	H	O	OH	H_2O	HO_2	C_2H_2	C_2H_4
9	10	11	12	13	14	15		
CO	CO_2	CH_3	CH_4	H_2CO	$C_6H_{12}O$	$C_{12}H_{24}$		

to dissociate (for example, O_2 starts to dissociate around 2000 K and is nearly completely dissociated by 4000 K at a pressure of 1 atm). From Fig. 3(B) one can see that the mass fractions of water and carbon dioxide (species 5 and 10) are approximately 0.21 and 0.30 respectively, which are markedly different from the complete combustion values calculated directly from Eq. 99 of 0.29 and 0.71. Given the drastic reduction in the presence of CO_2 as well as the reduction in H_2O (although not as dramatic), it can be inferred that at the given equilibrium temperature these two combustion products start to dissociate into more basic species such as carbon monoxide (CO, species 9) and OH (species 4). This dissociation process allows for the formation of O_2 *during combustion* and thus its presence does not reflect a fuel lean mixture but rather a combustion temperature too high to consider the complete combustion model an accurate assessment of the combustion process. Indeed, of this O_2 formed, some of it dissociates into O (species 3) as shown in Fig. 3(B) which is to be expected given the temperature (although clearly the O_2 dissociation process is not as complete as might be expected given the temperature, which is due partly to the pressure at which combustion is taking place. At a pressure of 1.5 MPa, which is approximately 15 atm, dissociation is reduced when compared to lower pressures at the same temperature).

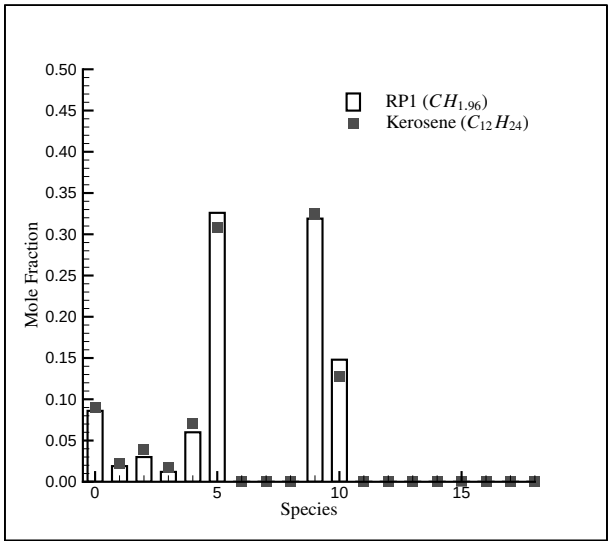

FIGURE 4. Equilibrium combustion results at an equivalence ratio of 1.33 for RP1, $\phi CH_2 + 1.5O_2 \rightarrow H_2O + CO_2$ (taken from Hill and Peterson)

This result is seen with other hydrocarbon fuels as well, as shown in Fig. 4. Here, the results (taken from Hill and Peterson) of an equilibrium combustion calculation are shown for RP1 ($CH_{1.96}$) which has approximately the same ratio of carbon to hydrogen as kerosene ($C_{12}H_{24}$). These results are for an equivalence ratio of 1.33 (which is approximately the equivalence ratio at which the peak equilibrium temperature is reached, see Fig. 3(A)) with an initial temperature and pressure of 298 K and 6.89 MPa respectively. As can be seen, the combustion of kerosene at the same conditions matches the results for RP1, with the *mole fraction* (as opposed to mass fraction as used in Fig. 3 (B)) of CO_2 being significantly depleted, CO amounts being elevated,

and residual O_2 being present despite the fact that the mixture is fuel rich.

Going back to the conditions for which the results in Fig. 3(B) are obtained, Fig. 5 shows the mass fractions of the various species over an increasing range of equivalence ratios, from a fuel lean mixture of $\phi = 0.5$ to a fuel rich mixture with $\phi = 4.5$. As can be seen, the mass fraction distribution at $\phi = 3$ exhibits a change in composition, from four species to two, as the decreasing amounts of both water and carbon dioxide have finally reached zero leaving only hydrogen and carbon monoxide. However past this point at an equivalence ratio of 3.5, there are again four species, only this time the new species are those arising out of the partial oxidization of kerosene, i.e., the kerosene is only partly broken down leaving some lighter unburned hydrocarbons behind such as C_2H_2 and C_2H_4. This sharp change in mixture composition, not merely changing the amounts of given species, but actually changing the species present in the mixture, is responsible for the sharp change in γ seen in Fig. 3(A) at an equivalence ratio of 3.

To summarize, the presence of residual O_2 at equivalence ratios of less than 3 and greater than 1 does not indicate a fuel lean mixture, but rather that the combustion process represented by Eq. 99 is no longer valid (as partial dissociation of the combustion products occurs due to the elevated temperature). Also, if one assumes that the combustion process occurs as follows (where the combustion products are now CO and H_2),

$$\phi C_{12}H_{24} + 6O_2 \longrightarrow 12CO + 12H_2 \tag{100}$$

then the $(\frac{f}{a})$ is 1/6 or 0.1667 on a molar basis or 0.8767 on a mass basis. Given molecular weights of 28.0104 kg/kmol and 2.01588 kg/kmol for CO and H_2 respectively this leads to mass fractions of 0.932 for CO and 0.067 for H_2 assuming Eq. 100. These are indeed the values in Fig. 5(F). And comparing this fuel to air (or oxygen in this case) ratio to the stoichiometric value determined from Eq. 99 of 0.2916 one realizes that $\frac{f}{a} = 0.8767$ is indeed 3 times this value, therefore $\phi = 3$. Thus at equivalence ratios higher than 3, the complete combustion model of Eq. 99 is totally inaccurate and must be replaced with Eq. 100.

4.3 Nozzle Design Results

The following nozzle designs are for a combustion mixture of kerosene ($C_{12}H_{24}$) and pure oxygen (O_2) at an equivalence ratio, ϕ, of one (based on the complete combustion reaction in Eq. 99),

$$\phi C_{12}H_{24} + 18O_2 \longrightarrow 12H_2O + 12CO_2$$

The combustion is assumed to occur at a constant pressure of 1.5 MPa while the total temperature at the end of the combustion process is assumed to be equal to the equilibrium combustion temperature. For an input fuel temperature of 300 K this yields a total temperature of 3533.55 K. The pertinent combustion variables are summarized in Table 7 while the resulting mixture composition on both a mass and mole fraction basis is shown in Fig. 6. The equilibrium combustion calculations consider a total of sixteen possible species as listed in Table 9.

TABLE 7.
Mixture Properties

Chamber Conditions	Value
Equivalence Ratio, ϕ	1
Fuel Input Temperature	300 K
Total Pressure	1.5 MPa
Post Combustion Equilibrium Temperature	3533.55 K
Post Combustion Specific Heat Ratio, γ	1.2175998
Post Combustion Mixture Molecular Weight	24.412 kg/kmol

For an exit Mach number of 5, Fig. 7(A) shows the inviscid contour created and the resulting final contour after being adjusted for the presence of the boundary layer (which is also shown

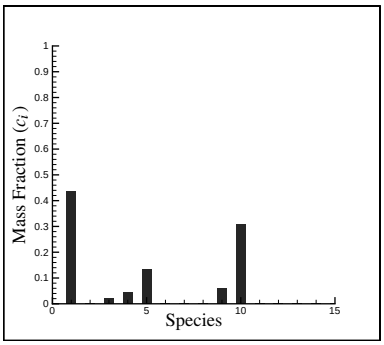

(a) $\phi = 0.5$

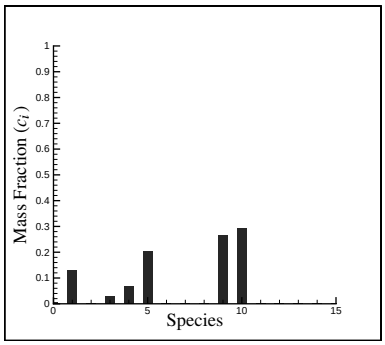

(b) $\phi = 1.0$

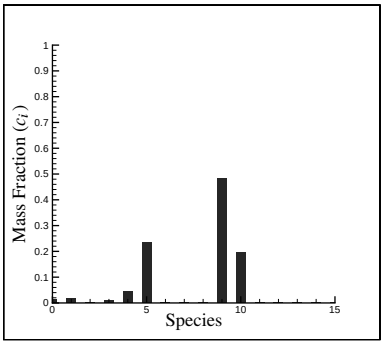

(c) $\phi = 1.5$

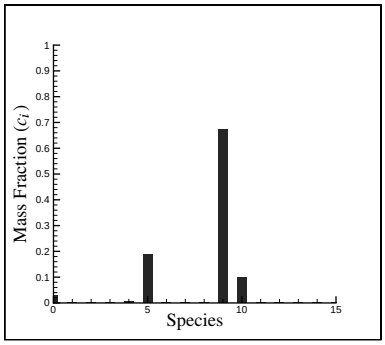

(d) $\phi = 2.0$

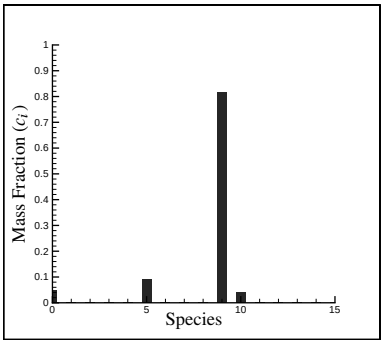

(e) $\phi = 2.5$

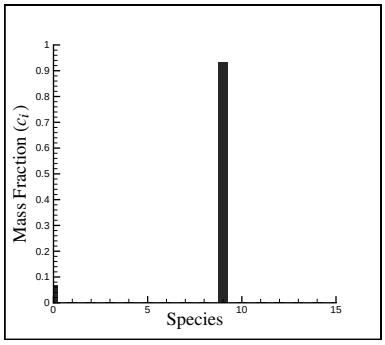

(f) $\phi = 3.0$

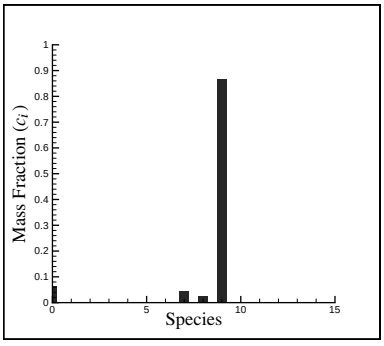

(g) $\phi = 3.5$

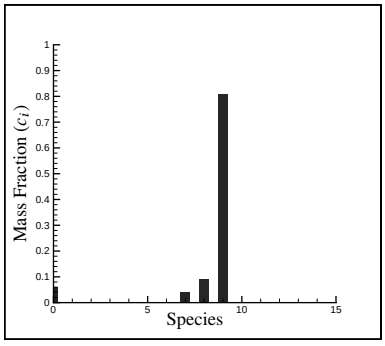

(h) $\phi = 4.0$

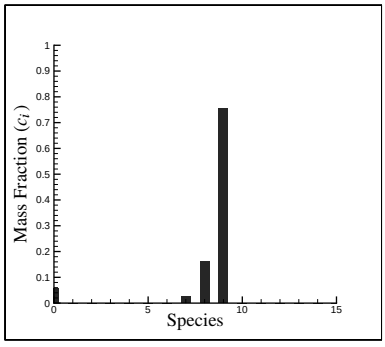

TABLE 8.
Nozzle Design Parameters

Nozzle Design Variable	Value
Maximum Expansion Angle, ω	10^o
Throat Radius	1 cm
Exit Mach Number, M_e	3, 4, 5
Wall Temperature	800 K
Mach Number at Combustion Chamber Exit	0.1
Subsonic Section Length (% of Supersonic Length)	25%

TABLE 9.
Species Map for Figure 6

0	1	2	3	4	5	6	7	8
H_2	O_2	H	O	OH	H_2O	HO_2	C_2H_2	C_2H_4
9	10	11	12	13	14	15		
CO	CO_2	CH_3	CH_4	H_2CO	$C_6H_{12}O$	$C_{12}H_{24}$		

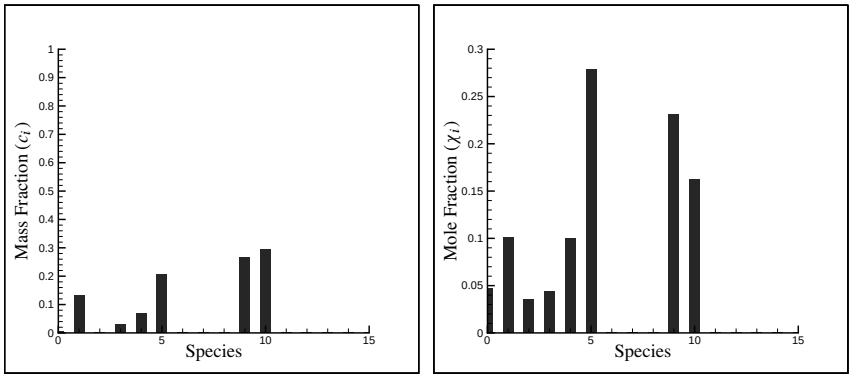

(a) Mass Fractions (b) Mole Fractions

FIGURE 6. Post combustion mixture composition entering nozzle

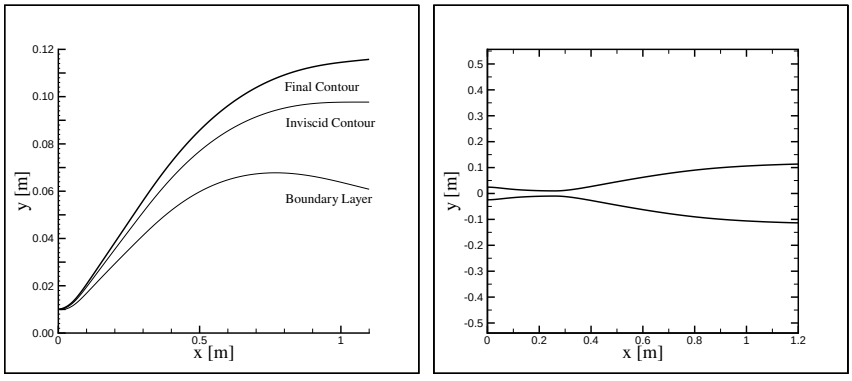

(a) Inviscid contour and boundary layer for $M_e = 5$ (b) Complete axisymmetric nozzle shape for $M_e = 5$

FIGURE 7. Axisymmetric Nozzle Design

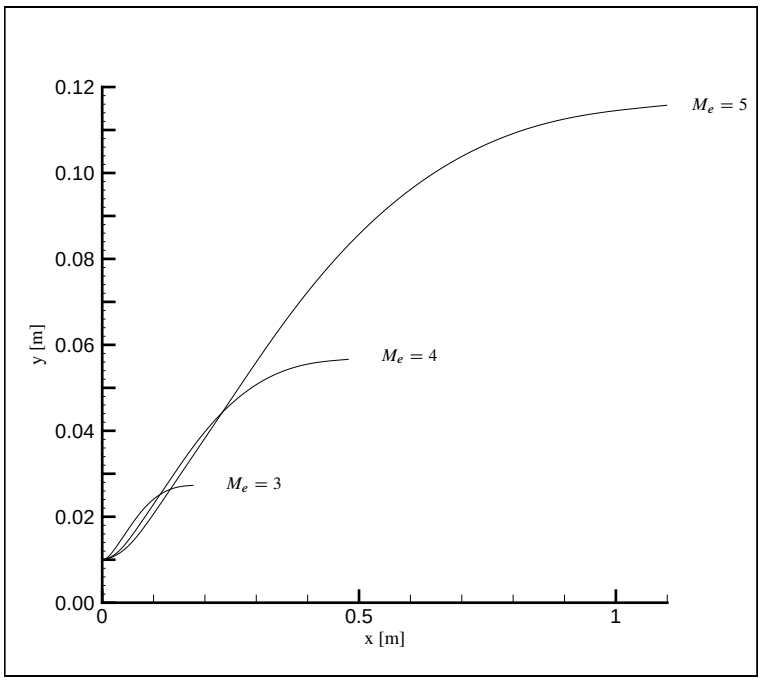

FIGURE 8. Nozzle designs for various exit Mach numbers

in the figure). As one can see, the resulting boundary layer at the nozzle exit is quite large which results in many cases in a truncation of the nozzle length to maximize the resulting high velocity core region. Adding a subsonic portion ahead of the throat with a length set at 25% of the diverging length and a chamber Mach number of 0.1 yields the nozzle shape shown in Fig. 7(B). Various nozzle designs are shown in Fig. 8 for nozzles with several different exit Mach numbers (while all other input variables remain constant).

4.4 Computational Results

The preceding nozzle design is used in an axisymmetric, implicit, steady state computational code (which uses the Wilcox $k - \omega$ two equation turbulence model) to verify the predictions made (this code is called WARP, developed by B. Parent). A uniform grid with 150 points in the downstream direction (parallel to the nozzle axis) and 50 points in the cross stream direction is used. Figure 9 shows the Mach number along the nozzle centreline as compared to both the desired Mach number distribution (as found from the method previously described) and the isentropic area/mach number relation (Eq. 97).

As can be seen, although the computed Mach number at the exit of approximately 5.6 is slightly higher than the design Mach number of 5, it does follow the desired contour as the velocity is increased from Mach one at the throat through the expanding portion of the nozzle. In fact, as can be seen up to a distance of approximately 0.5 m, the predicted increase in Mach number follows the desired increase quite well. It is also noted that the pre-specified Mach number distribution also follows the isentropic relation very closely, which is to be expected given the manner in which the nozzle is designed. In using the two dimensional method of characteristics for irrotational flow, from Crocco's theorem one can conclude that since the conditions at the end of the combustion chamber are assumed uniform (i.e. constant enthalpy everywhere) then the flow must be homentropic (constant entropy everywhere). If the flow is homentropic, then it must also be isentropic (entropy is constant along a given streamline, but not necessarily constant *between* streamlines) and hence Eq. 97 must apply.

The slight decrease in Mach number in the computational solution near the nozzle exit is caused by an increase in temperature at this location, as can be seen in Fig. 10. Near the nozzle exit, the slope of the wall is nearly parallel with the nozzle axis and is thus approximately

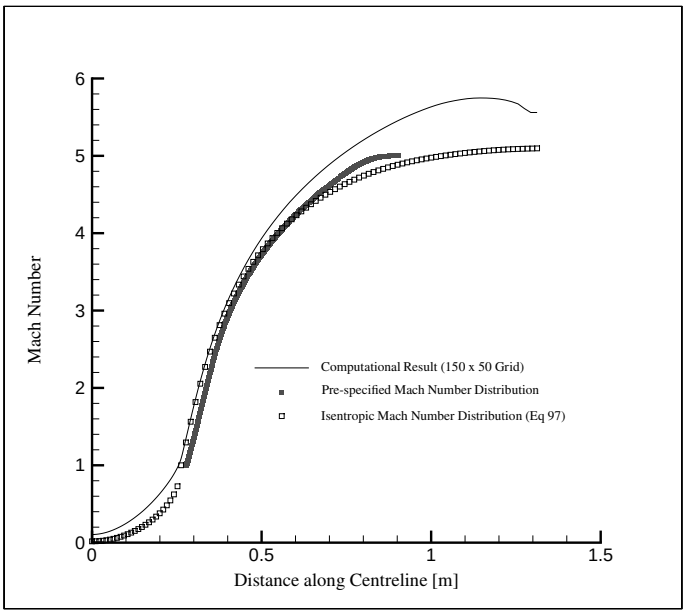

FIGURE 9. Mach number along nozzle centreline

a constant area duct. Viscous effects in a constant area duct cause the temperature to rise and the Mach number to tend to unity, thereby causing the decrease in Mach number and the increase in temperature seen at this location. Also shown in Fig. 10 is the isentropic temperature relation which follows the computed solution very well until approximately the 0.4 m location, at which point the real gas effects become significant thereby reducing the accuracy of assuming isentropic flow. It is also noted that the isentropic result shows no temperature increase at the nozzle exit, reinforcing the fact that the computed temperature rise is indeed a viscous effect.

Also shown in Fig. 10 is the value for the ratio of specific heats throughout the nozzle. At the combustion chamber exit it starts at the value found from the equilibrium combustion calculations. During the nozzle design, this value is assumed constant throughout the expansion process and as can be seen from the computational results, this assumption is fairly accurate within the subsonic portion of the nozzle. However, as the expansion process continues past a distance downstream of approximately 0.4 m (Fig. 10) the constant γ assumption starts to become less valid. This accounts for the differences in the computed mach number in the latter portions of the nozzle as compared to the pre-specified distribution. This change in γ is also responsible for the difference between the pre-specified and isentropic Mach number and temperature distributions shown in Figs. 9 and 10, since for the isentropic results γ is held constant at the combustion chamber exit value (approximately 1.22).

Figure 11 shows the Mach contours in within the nozzle. Here one can see the approximate shape of the boundary layer (as these contours depend on velocity *and* temperature, hence although the decreasing velocity is shown in the Mach number contours near the wall, this decrease is altered to some extent by the increasing temperature as one approaches the wall as well). Also, one can see the bubble of increased velocity along the nozzle centreline above the design Mach number of 5.

A Two Dimensional Method of Characteristics (Irrotational Flow)

A.1 Derivation of Characteristic and Compatibility Equations

The gas dynamic equation (Eq. 31), stated again here for convenience, can be rewritten as follows.

$$\boldsymbol{q} \cdot \nabla(\frac{q^2}{2}) - a^2(\nabla \cdot \boldsymbol{q}) = 0$$

Taking $\boldsymbol{q} = u + v$ where u and v are the velocities parallel and normal to the axisymmetric axis respectively, then the dot product $\nabla \cdot \boldsymbol{q}$ can be expressed in cylindrical co-ordinates as,

$$\nabla \cdot \boldsymbol{q} = \frac{\partial u}{\partial x} + \frac{\partial v}{\partial r} + \frac{v}{r} \tag{101}$$

Substituting this into the gas dynamic equation yields,

$$\boldsymbol{q} \cdot \nabla(\frac{q^2}{2}) - a^2\Big\{\frac{\partial u}{\partial x} + \frac{\partial v}{\partial r} + \frac{v}{r}\Big\} = 0$$

Expanding out the first term one can write,

$$(u+v)\cdot\Big\{\frac{1}{2}(\frac{\partial q^2}{\partial x} + \frac{\partial q^2}{\partial r})\Big\} - a^2\Big\{\frac{\partial u}{\partial x} + \frac{\partial v}{\partial r} + \frac{v}{r}\Big\} = \frac{1}{2}(u\frac{\partial q^2}{\partial x} + v\frac{\partial q^2}{\partial r}) - a^2\Big\{\frac{\partial u}{\partial x} + \frac{\partial v}{\partial r} + \frac{v}{r}\Big\} = 0$$

Given the definition of q one can write for the derivative of its square,

$$\frac{\partial q^2}{\partial x} = \frac{\partial}{\partial x}(u^2 + v^2) = 2(u\frac{\partial u}{\partial x} + v\frac{\partial v}{\partial x})$$

and

$$\frac{\partial q^2}{\partial r} = \frac{\partial}{\partial r}(u^2 + v^2) = 2(u\frac{\partial u}{\partial r} + v\frac{\partial v}{\partial r})$$

which when substituted into the gas dynamic equation yields,

$$u(u\frac{\partial u}{\partial x} + v\frac{\partial v}{\partial x}) + v(u\frac{\partial u}{\partial r} + v\frac{\partial v}{\partial r}) - a^2(\frac{\partial u}{\partial x} + \frac{\partial v}{\partial r} + \frac{v}{r}) = 0$$

If the flow is assumed irrotational then one also write the relation

$$\frac{du}{dr} - \frac{dv}{dx} = 0 \tag{102}$$

which allows the above to be simplified to,

$$(u^2 - a^2)\frac{du}{dx} + (v^2 - a^2)\frac{dv}{dr} + 2uv\frac{du}{dr} - \frac{a^2 v}{r} = 0 \tag{103}$$

Equations 102 and 103 form the basis of the two dimensional axisymmetric method of characteristics, as from these one can develop both the compatibility and characteristic equations. Starting by multiplying Eq. 103 by σ_1 and Eq. 102 by σ_2 (where σ_1 and σ_2 are arbitrary functions to be determined later) and summing the resulting equations to zero yields,

$$\sigma_1(u^2 - a^2)\frac{du}{dx} + \sigma_1(v^2 - a^2)\frac{dv}{dr} + \sigma_1 2uv\frac{du}{dr} - \sigma_1\frac{a^2 v}{r} + \sigma_2\frac{du}{dr} - \sigma_2\frac{dv}{dx} = 0$$

which after grouping the derivatives of a single velocity together and rearranging yields,

$$\sigma_1(u^2 - a^2)\Big\{\frac{\partial u}{\partial x} + \frac{\sigma_1 2uv + \sigma_2}{\sigma_1(u^2 - a^2)}\frac{\partial u}{\partial r}\Big\} - \sigma_2\Big\{\frac{\partial v}{\partial x} + \frac{\sigma_1(v^2 - a^2)}{-\sigma_2}\frac{\partial v}{\partial r}\Big\} - \sigma_1\frac{a^2 v}{r} = 0 \tag{104}$$

Since one of the properties enforced on the dependent variables ($u(x, y)$ and $v(x, y)$) is that they be continuous functions across the characteristic curves one can write,

$$\frac{du}{dx} = \frac{\partial u}{\partial x} + \lambda\frac{\partial u}{\partial r} \qquad \text{and} \qquad \frac{dv}{dx} = \frac{\partial v}{\partial x} + \lambda\frac{\partial v}{\partial r}$$

where $\lambda = \frac{dy}{dx}$ and is hence the slope of the characteristic in the physical plane along which the total derivatives can be defined as above. Therefore the characteristic curves for Eq. 104 must have slopes of,

$$\lambda = \frac{\sigma_1 2uv + \sigma_2}{\sigma_1(u^2 - a^2)} \qquad \text{and} \qquad \lambda = \frac{\sigma_1(v^2 - a^2)}{-\sigma_2} \tag{105}$$

which then allows Eq. 104 to be written as,

$$\sigma_1(u^2 - a^2)du - \sigma_2 dv - \sigma_1 \frac{a^2 v}{r} dx = 0 \tag{106}$$

Equation 106 is the compatibility equation for axisymmetric irrotational flow, as defined by Eqs. 102 and 103. However, for this equation to be of use, the arbitrary functions must be phrased in terms of known quantities. Therefore, rewriting Eqs. 105 in matrix form gives,

$$\begin{bmatrix} (u^2 - a^2)\lambda - 2uv & -1 \\ (v^2 - a^2) & \lambda \end{bmatrix} \begin{bmatrix} \sigma_1 \\ \sigma_2 \end{bmatrix} = 0$$

Taking the determinant of the co-efficient matrix and setting this equal to zero yields,

$$(u^2 - a^2)\lambda^2 - 2uv\lambda + (v^2 - a^2) = 0$$

which can be solved using the quadratic formula to give the result,

$$\lambda_\pm = \frac{uv \pm a^2\sqrt{M^2 - 1}}{u^2 - a^2} \tag{107}$$

where the $+$ sign refers to the positive square root and the $-$ refers to the negative. Since λ is the slope of the characteristic in the physical plane, this means that for flows where $M > 1$ there exist two distinct characteristic curves. Equation 107 can be rephrased by noting that,

$$\theta = \tan^{-1}(\frac{v}{u}) \qquad , \qquad u = q\cos\theta \qquad , \qquad v = q\sin\theta$$

while from the Mach triangle one can write (where α is the Mach angle),

$$\alpha = \sin^{-1}(\frac{1}{M}) \qquad , \qquad \tan\alpha = \frac{1}{\sqrt{M^2 - 1}}$$

Substituting these relations into Eq. 107 yields,

$$\lambda_\pm = \frac{(q\cos\theta)(q\sin\theta) \pm a^2(\frac{1}{\tan\alpha})}{(q\cos\theta)^2 - a^2}$$

while dividing through by q^2 and noting that $\frac{a^2}{q^2} = M^{-2}$ yields,

$$\lambda_\pm = \frac{\cos\theta\sin\theta \pm \frac{1}{\tan\alpha}M^{-2}}{\cos^2\theta - M^{-2}}$$

Using the definition of the Mach angle allows the above to be simplified to,

$$\lambda_\pm = \frac{\cos\theta\sin\theta \pm \cos\alpha\sin\alpha}{\cos^2\theta - \sin^2\alpha}$$

The above can be further simplified by making use of trigonometric identities allowing an alternate form for λ to be expressed as,

$$\boxed{\lambda_\pm = (\frac{dy}{dx})_\pm = \tan(\theta \pm \alpha)} \tag{108}$$

Equation 108 is the characteristic equation for axisymmetric irrotational flow. Having determined the characteristic equation one can return to the compatibility equation to eliminate the arbitrary functions σ_1 and σ_2 as follows. From Eqs. 105 one can express σ_2 as,

$$\sigma_1\Big\{(u^2-a^2)\lambda-2uv\Big\}=\sigma_2=-\frac{\sigma_1(v^2-a^2)}{\lambda}$$

Although not immediately apparent, these two equations are not independent and thus either one can be substituted back into Eq. 106 to eliminate both arbitrary functions,

$$\sigma_1(u^2-a^2)du-\Big\{\sigma_1\Big[(u^2-a^2)\lambda-2uv\Big]\Big\}dv-\sigma_1\frac{a^2v}{r}dx=0$$

which after dividing through by σ_1 yields,

$$\boxed{(u^2-a^2)du_\pm-\Big[(u^2-a^2)\lambda_\pm-2uv\Big]dv_\pm-\tfrac{a^2v}{r}dx_\pm=0} \tag{109}$$

where if the positive value of λ is used, then Eq. 109 applies along the C_+ characteristic and hence all values du, dv, and dx apply to this curve. It is noted that if the other definition of σ_2 is substituted into Eq. 106 to eliminate the arbitrary values, then a slightly different form of the compatibility equation is obtained. However, this merely produces an alternate form of the same equation, not an independent relation that is also applicable along the characteristic.

A.2 Numerical Implementation of the Method of Characteristics

Having derived the characteristic (Eq. 108) and compatibility (Eq. 109) equations, one can now use these in a numerical integration scheme to completely determine a supersonic flow field. If one defines the following parameters,

$$Q=u^2-a^2 \qquad R=2uv-Q\lambda \qquad S=\frac{a^2v}{y} \tag{110}$$

then the characteristic and compatibility equations can be written in finite difference form as,

$$\Delta y_\pm=\lambda_\pm\Delta x_\pm \tag{111}$$

$$Q_\pm\Delta u_\pm+R_\pm\Delta v_\pm-S_\pm\Delta x_\pm=0 \tag{112}$$

If one considers a line along which the flow field in completely known, then from two points (points 1 and 2) along this line, two opposing characteristic curves will intersect each other at some unknown point 4. Using these three points, one can use Eq. 111 to determine the intersection point (4) as follows,

$$y_4=y_1+\lambda_-(x_4-x_1)$$

while from the other characteristic,

$$\boxed{y_4=y_2+\lambda_+(x_4-x_2)} \tag{113}$$

thus yielding for x_4,

$$\boxed{x_4=\tfrac{y_1-y_2-\lambda_-x_1+\lambda_+x_2}{\lambda_+-\lambda_-}} \tag{114}$$

Once x_4 is found, expression in Eq. 113 can be used to completely determine the physical location of the intersection point of the two opposing characteristic curves emanating from points 1 and 2. To determine the flow properties at this point one can make use of Eq. 112 by calculating along each characteristic,

$$\begin{aligned}T_-&=S_-(x_4-x_1)+Q_-u_1+R_-v_1\\ T_+&=S_+(x_4-x_2)+Q_+u_2+R_+v_2\end{aligned} \tag{115}$$

which then from Eq. 112 along the C_- characteristic,

$$Q_-(u_4 - u_1) + R_-(v_4 - v_1) - S_-(x_4 - x_1) = 0$$

while rearranging and substituting Eq. 115 yields,

$$Q_-u_4 + R_-v_4 = S_-(x_4 - x_1) + Q_-u_1 + R_-v_1 = T_-$$

therefore,

$$\boxed{v_4 = \frac{T_- - Q_-u_4}{R_-}} \tag{116}$$

Along the C_+ characteristic one can write,

$$Q_+u_4 + R_+v_4 = S_+(x_4 - x_2) + Q_+u_2 + R_+v_2 = T_+$$

which when Eq. 116 is used to replace v_4 yields a solution for u_4,

$$Q_+u_4 + R_+\left\{\frac{T_- - Q_-u_4}{R_-}\right\} = T_+$$

$$R_+T_- - R_+Q_-u_4 = R_-T_+ - R_-Q_+u_4$$

$$\boxed{u_4 = \frac{R_+T_- - R_-T_+}{R_+Q_- - R_-Q_+}} \tag{117}$$

with the velocity components found from Eqs. 116 and 117 at the intersection point 4, one has now determined the flow conditions at a point further downstream (or upstream, depending on the direction chosen) of the original line at which the flow conditions are known (noting that each subsequent intersection point must still lie within a supersonic flow field).

The accuracy of the characteristic mesh being built can be improved by employing a predictor-corrector scheme to the solution of point 4 as follows. After having completely determined the intersection point as outlined above (the predictor step), the procedure is repeated using the average values of the flow properties along each characteristic (between points 1 and 4 and points 2 and 4) to recalculate the values found from Eqs. 110 and 115 which are then used to find a new intersection point 4. This procedure can be repeated until a specified tolerance level is reached.

$$\begin{array}{lll} y_-^{corr} = \frac{1}{2}(y_1 + y_4) & u_-^{corr} = \frac{1}{2}(u_1 + u_4) & v_-^{corr} = \frac{1}{2}(v_1 + v_4) \\ y_+^{corr} = \frac{1}{2}(y_2 + y_4) & u_+^{corr} = \frac{1}{2}(u_2 + u_4) & v_+^{corr} = \frac{1}{2}(v_2 + v_4) \end{array} \tag{118}$$

References

[1] DUDEBOUT, R., *Axisymmetric Hypersonic Contoured Nozzle Design*, Master's thesis, University of Toronto, Institute for Aerospace Studies, August 1989.

[2] ZUCROW, M. J. AND HOFFMAN, J. D., *Gas Dynamics:Multidimensional Flow*, Vol. 2, John Wiley and Sons, 1977.

[3] ZUCROW, M. J. AND HOFFMAN, J. D., *Gas Dynamics*, Vol. 1, John Wiley and Sons, 1976.

[4] SIVELLS, J. C., "Aerodynamic Design of Axisymmetric Hypersonic Wind-Tunnel Nozzles," *Journal of Spacecraft*, November 1970, pp. 1292–1299.

[5] FOELSCH, K., "The Analytical Design of an Axially Symmetric Laval Nozzle for a Parallel and Uniform Jet," *Journal of the Aeronautical Sciences*, March 1949, pp. 161–188.

[6] KLIEGEL, J. R. AND LEVINE, J. N., "Transonic Flow in Small Throat Radius of Curvature Nozzles," *AIAA Journal*, Vol. 7, No. 7, July 1969, pp. 1375–1378.

[7] SIMEONIDES, G., "The Aerodynamic Design of Hypersonic Contoured Axisymmetric Nozzles Including Real Gas Effects," Tech. rep., von Karman Institute for Fluid Dynamics, Rhode Saint Genese Belgium, March 1987, Technical Memorandum 43.

[8] EVVARD, J. C. AND MASLEN, S. H., "Three-Dimensional Supersonic Nozzles and Inlets of Arbitrary Exit Cross Section," Tech. rep., National Advisory Committee for Aeronautics, Lewis Flight Propulsion Laboratory, April 1952, NACA TN 2688.

[9] EDENFIELD, E. E., "Design of a High Reynolds Number Mach Number 8 Contoured Nozzle for the Hypersonic Wind Tunnel (F)," Tech. rep., Arnold Engineering Development Centre, Arnold Air Force Station, Tennessee, August 1972, AEDC-TR-72-48.

[10] SISLIAN, J. P., "Airbreathing Propulsion Notes," University of Toronto Institute for Aerospace Studies.

[11] Jr., W. C. G., editor, *Combustion Chemistry*, chap. 2, Springer-Verlag, 1984, pp. 37–125.

[12] SVEHLA, R. A., "Estimated Viscosities and Thermal Conductivities of Gases at High Temperatures," Tech. rep., NASA, 1962.

[13] Launder, B. E., editor, *Studies in Convection: Theory, Measurement and Applications*, Vol. 2, chap. Calculation of Chemically Reacting Flows with Complex Chemistry, Academic Press, 1977, pp. 191–221.

[14] MCBRIDE, B. J., GORDON, S., AND RENO, M. A., "Coefficients for Calculating Thermodynamic and Transport Properties of Individual Species," Tech. Rep. NASA TM 4513, NASA, October 1993.

[15] STEWART, J., *Calculus*, Brooks/Cole Publishing Company, McMaster University, 2nd ed., 1991.

[16] HILL, P. AND PETERSON, C., *Mechanics and Thermodynamics of Propulsion*, chap. 12, Addison-Wesley, 2nd ed., 1992, pp. 569–614.

[17] FUSINA, G., *An Investigation of Standing Oblique Detonation Waves with Hydrogen-Air Equilibrium Chemical Reactions*, Master's thesis, University of Toronto, Institute for Aerospace Studies, April 1995.

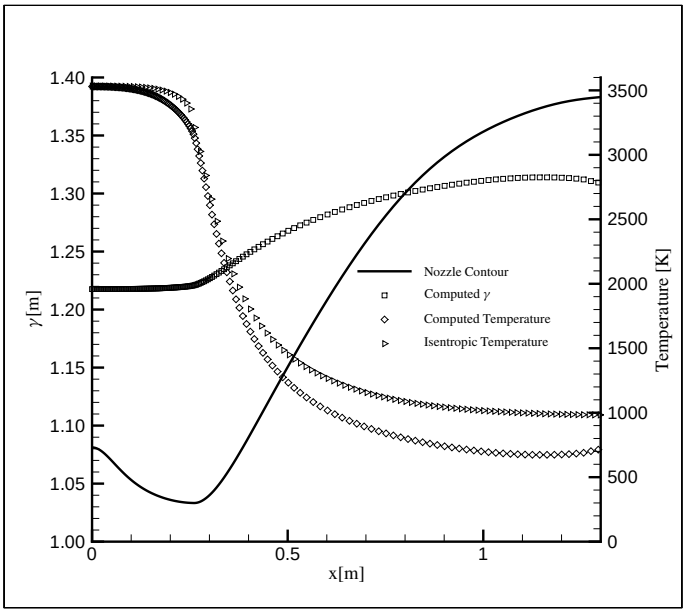

FIGURE 10. Variation of Temperature and Specific Heat Ratio along Nozzle Centreline

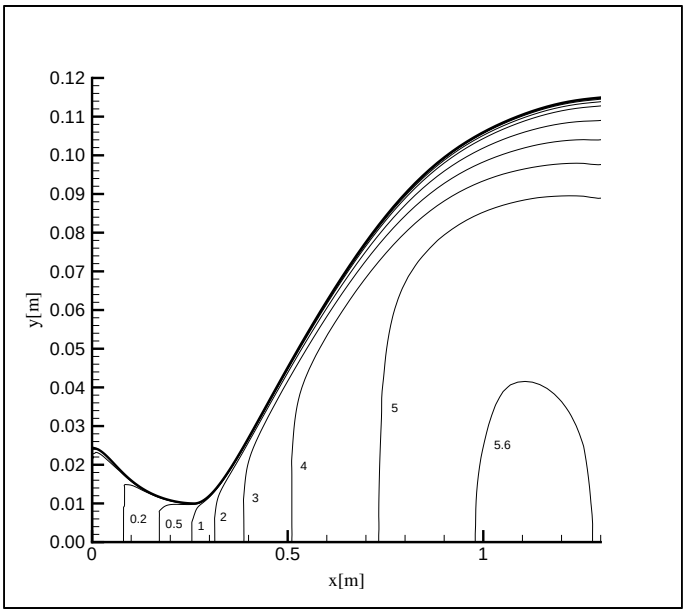

FIGURE 11. Mach contours within nozzle